Chromatin activity of IκBα mediates the exit from naïve pluripotency

Luis G. Palma[1,2,3,δ], Daniel Álvarez-Villanueva[1,4,δ], María Maqueda[1,2,3], Mercedes Barrero[5], Arnau Iglesias[1,2,3], Joan Bertran[6], Damiana Álvarez-Errico[2], Carlos A. García-Prieto[2], Cecilia Ballaré[5], Virginia Rodriguez-Cortez[2], Clara Bueno[2], August Vidal[4], Alberto Villanueva[7], Pablo Menéndez[2,3,8,9,10], Gregoire Stik[2], Luciano Di Croce[5,10,11], Bernhard Payer[5,11], Manel Esteller[2,3,10,12], Lluís Espinosa[1,3,*] & Anna Bigas[1,2,3,*]

[1]Program in Cancer Research. Hospital del Mar Research Institute, Barcelona, Spain.

[2]Josep Carreras Leukemia Research Institute, Barcelona Spain.

[3]Centro de Investigación Biomédica en Red Cancer (CIBERONC), Madrid, Spain.

[4]Institut Investigació Biomèdica de Bellvitge (IDIBELL), L'Hospitalet de Llobregat, Barcelona, Spain.

[5]Centre for Genomic Regulation (CRG), The Barcelona Institute of Science and Technology, Barcelona, Spain.

[6]Faculty of Sciences, Technology and Engineering, Universitat de Vic - Universitat Central de Catalunya, Vic 08500 Spain

[7]Catalan Institute of Oncology (ICO/IDIBELL), L'Hospitalet de Llobregat, Barcelona, Spain.

[8]Spanish Network for Advanced Therapies (RICORS-TERAV). Carlos III Health Institute (ISCIII), Spain.

[9]Department of Biomedicine. University of Barcelona, Spain.

[10]Institucio Catalana de Recerca i Estudis Avançats (ICREA), Barcelona, Spain.

[11] Universitat Pompeu Fabra, Barcelona, Spain.

[12]Physiological Sciences Department, School of Medicine and Health Sciences, University of Barcelona (UB), Barcelona, Catalonia, Spain.

[δ]These authors contributed equally

Keywords: IκBα, NFKBIA, NF-κB, DNA Methylation, Polycomb, Embryonic Stem Cells, Pluripotency Exit, Germ Layer Specification,

**Corresponding authors:*

28 Anna Bigas and Lluis Espinosa

29 Cancer Research Program. CIBERONC.

30 Hospital del Mar Research Institute

31 Doctor Aiguader 88, 08003, Spain.

32 Tel: +34 933160440; email: abigas@researchmar.net; lespinosa@researchmar.net

33 **Summary**

34 Maintenance of pluripotency is a multifactorial process in which NF-κB is a negative regulator. Our
35 previous work identified a chromatin role for IκBα, the master regulator of NF-κB signaling, that is
36 critical for the proper regulation of various tissue stem cells. Here, we found that IκBα accumulates
37 specifically in the chromatin fraction of pluripotent embryonic stem cells. IκBα depletion does not
38 affect NF-kB-dependent transcription, but causes a profound epigenetic rewiring in pluripotent stem
39 cells, including alterations in H3K27me3, a histone mark catalyzed by Polycomb repression complex
40 2. Chromatin changes induced by IκBα depletion affect a subset of pluripotency genes and are
41 associated with altered gene transcription. At the cellular level, IκBα-deficient embryonic stem cells
42 are arrested in a naive pluripotency state when cultured in serum/LIF conditions and fail to exit
43 pluripotency under differentiation conditions. By constructing separation-of-function mutants, we
44 show that the effects of IκBα in regulating stem cell pluripotency are NF-κB-independent, but mainly
45 rely on its chromatin-related function. Taken together, our results reveal a novel mechanism by which
46 IκBα participates in the regulation of the pluripotent state of embryonic stem cells and shed light on
47 the interplay between inflammatory signals and the regulation of pluripotency.

INTRODUCTION

Embryonic Stem Cells (ESCs) pluripotency is characterized by the capacity to generate all somatic and germline lineages both *in vitro* and *in vivo*, depending on the culture conditions. When cultured in serum plus Leukemia Inhibitory Factor (LIF) (Serum/LIF), murine ESCs (mESCs) include cells interconverting to different metastable states [1] that either resemble preimplantation blastocyst (naïve pluripotency) or post-implantation (primed pluripotency) embryonic stages [2–5]. The heterogeneity of mESCs in Serum/LIF is reduced by culturing them in the presence of GSK3β and MEK1/2 inhibitors (CHIR99021 and PD0325901, respectively) along with LIF (2i/LIF). Under these conditions, mESCs enter a ground state of naïve pluripotency characterized by self-renewal activity while suppressing any pro-differentiating signals [6,7]. This pluripotent state closely resembles the inner cell mass of the E4.0 mouse preimplantation blastocyst [8]. After implantation, pluripotent capability of the mouse embryo (E5.5) becomes restricted to Epiblast Stem Cells (EpiSCs), which represent a primed pluripotent state, characterized by coexpression of pluripotency and lineage specification markers [9,10]. EpiSCs can give rise to cells from the three germ layers (endoderm, mesoderm and ectoderm), albeit their contribution to chimeras or to germ cells is greatly compromised [4,11]. EpiSCs can be derived *in vitro* from naïve pluripotent cells when cultured in a medium supplemented with Nodal and fibroblast growth factor (FGF) [12]. Different epigenetic features distinguish naïve from primed pluripotent states [13], such as changes in the X chromosome inactivation in female cells [12,14], histone post-translational modifications [10] or a global DNA hypomethylation profile observed in naïve pluripotent stem cells [15–17]. These epigenetic changes are a prerequisite for the subsequent activation of gene circuits associated with pluripotency exit and germ layer specification [9,10]. Crucial regulatory elements for the transition from naïve to primed pluripotency state are located in distal DNA regions or enhancers to facilitate the resolution toward the primed state [18,19]. Therefore, identifying novel players to fine-tune the equilibrium between ground and primed states is crucial for preserving both pluripotency stability and differentiation capability in mESCs.

There is now strong evidence that inflammatory signals are critical for stem cell development [20–22], with NF-κB being the main effector. Different strategies to inhibit or attenuate NF-κB in ESCs lead to increase pluripotency gene expression and impair cell differentiation [23,24], or it facilitates reprogramming to induced pluripotent stem cells (iPSC) [25]. Canonical NF-κB signaling is triggered by the IKK kinase complex, which induce the phosphorylation and subsequent degradation of the NF-κB inhibitor, IκBα, leading to nuclear translocation of the NF-κB factors (e.g. p50/p65) [26]. However, we have previously identified a nuclear IκBα function, which is critical for tissue stem cell homeostasis and the proper differentiation of epidermal, intestinal and hematopoietic stem cells [27–30]. IκBα chromatin function is mediated by the interaction with histone deacetylases (HDACs), core elements of the Polycomb Repressor Complex 2 (PRC2) and histone H2A and H4 [27,29,31].

86 We have now investigated the role of IκBα in the context of pluripotent stem cells. Whereas
87 cytoplasmic IκBα is detected in the different states and its levels decrease after
88 differentiation, in agreement with NF-κB activity as a promoter of differentiation, we
89 specifically detected chromatin-bound IκBα in the naïve pluripotent stem cells. Importantly,
90 IκBα depletion in ESCs did not affect NF-κB activity but it stabilizes the naïve (2i/LIF-like) state
91 of pluripotency under Serum/LIF conditions, displaying an epigenetic rewiring, including
92 changes in the PRC2-dependent H3K27me3 histone mark and impacting in proximal and distal
93 regulation of pluripotent genes. Using a new Separation-Of-Function (SOF) IκBα mutants[32],
94 we have now definitively demonstrated that chromatin-bound IκBα is required for naïve
95 pluripotency exit of mESCs in an NF-κB-independent manner. Overall, we identified IκBα as a
96 novel key player in the regulation of the exit from naïve-to-primed pluripotency and essential
97 for the activation of gene programs involved in germ layer specification.

98 **RESULTS**

99 **IκBα and NF-κB have opposite expression dynamics in naïve pluripotent cells**

100 Due to the prominent role of NF-κB signaling in mESCs regulation, we analyzed the expression
101 pattern of the different NF-κB members including the IκB inhibitors in the three defined
102 pluripotent stages: ground state of naïve pluripotency (2i/LIF), naïve pluripotency
103 (Serum/LIF), and primed pluripotency (Epiblast Stem Cells or EpiSCs) [5] (Figure 1A). In
104 agreement with NF-κB being a pro-differentiation factor, canonical NF-κB inhibitors including
105 IκBα (*Nfkbia*), IκBβ (*Nfkbib*) and IκBε (*Nfkbie*) were all expressed in the naïve pluripotency
106 state (both 2i/LIF and Serum/LIF), with *Nfkbia* levels gradually reduced upon naïve
107 pluripotency exit towards EpiSCs (Figure 1B). In contrast, *Rela, Nfkb1 and Nfkb2* genes,
108 codifying for the NF-κB factors p65/RelA, p105 and p100, respectively, showed opposite
109 expression dynamics increasing the levels in EpiSCs (Figure 1C). We further characterized the
110 distribution of IκBα in the cytoplasm, nucleus and chromatin fractions of the three states of
111 pluripotency (Figure 1D). Total IκBα protein levels correlated with the detected RNA levels in
112 the three different cellular states being highest in the 2i/LIF condition (Figure 1B), with a large
113 accumulation in the cytoplasm. A fraction of IκBα protein was detected in the chromatin of
114 naïve pluripotent cells, being highest in cells cultured in Serum/LIF conditions compared to
115 2i/LIF and absent in the EpiSCs. (Figure 1D). The dynamics of IκBα RNA and protein levels from
116 naïve pluripotent ESCs to EpiSCs was further corroborated by analysis of an additional
117 database that includes both naïve and primed pluripotent states[33] (Figure 1E).

118 Next, we studied IκBα expression in differentiated embryoid bodies (EBs) from mESCs
119 (Serum/LIF) (see materials and methods) and analyzed the expression levels of different
120 pluripotency, differentiation-linked, and NF-κB genes by RNA sequencing. *Nfkbia* (IκBα gene)
121 was expressed at higher levels specifically in mESCs (Serum/LIF) whereas cells undergoing
122 differentiation (48h and 96h) displayed a reduction in its expression levels (Figure 1F). The
123 expression pattern of *Nfkbia* was similar to the pluripotency genes whereas most of the NF-
124 κB genes were upregulated upon differentiation, showing an analogous expression dynamics
125 as developmental genes, as previously described [24]. Previous reports have demonstrated that
126 chromatin-bound IκBα modulates PRC2 activity in different adult stem cell models [27]. Notably,
127 we observed that most of the Polycomb target genes follow a similar expression pattern of
128 *Nfkbia* and pluripotency, with higher expression in mESCs (Figure 1F).

129 Taken together, these data show that, unlike the other NF-kB inhibitors and target genes, the
130 expression of *Nfkbia* is high in the naive pluripotent state, with IκBα protein present in the
131 cytoplasm and chromatin of naive pluripotent cells. Moreover, whereas canonical NF-κB
132 subunits are primarily absent, we detected several Polycomb elements expressed in mESCs.

133 **IκBα is required in mESCs to exit the naïve pluripotency state**

134 To investigate the functional implication of IκBα in naïve pluripotency, we knocked-out (KO)
135 IκBα protein in mESCs by CRISPR-Cas9 (IκBα-KO mESCs) (Figure S1A and materials and
136 methods). Notably, IκBα-KO mESCs have an impaired ability to undergo differentiation and
137 cannot properly switch off the pluripotency program after 216h (9 days) of pro-differentiation
138 signals, as it is demonstrated by high levels of pluripotency markers OCT3/4 and NANOG (Fig
139 2A and Fig S1C), higher number of alkaline phosphatase cells (Fig 2B and Fig S1D) and higher
140 percentage of SSEA-1^{+} cells (Fig S1C) within the 216h EBs. These results were also supported
141 by the detection of increased expression level of the naïve pluripotency genes *Pou5f1 (Oct3/4*
142 *gene), Gbx2, Klf2, Sox2, Zfp42 (Rex1)* and *Nanog* in IκBα KO EBs after 216h of differentiation
143 (Figure S1F) and lower differentiation (Figure S1G).

144 To shed light into the molecular mechanisms governing the differentiation impairment in IκBα
145 KO EBs, we performed RNA-seq of IκBα WT and IκBα KO mESCs in the first stages of the
146 embryoid body differentiation. Analysis of the data indicated that IκBα KO EBs cannot
147 successfully evolve towards differentiation trajectories, as shown by principal component
148 analysis (PCA) of IκBα-WT and IκBα-KO EBs at 48h and 96h in differentiation media (Figure
149 2C). Analysis of naïve pluripotency markers at 96h (*Gab1, Sox2, Esrrb, Zfp42, Dppa4, Klf2,*
150 *Prdm14, Klf4, Tfcp2l1*) also showed higher expression levels in IκBα KO compared to their IκBα
151 WT counterparts (Figures 2D and S1C). Defective differentiation capacity of IκBα KO EBs
152 involved programs associated with specification of all 3 germ layers (endoderm, mesoderm,
153 and ectoderm) (Figure 2E). Moreover, IκBα KO EBs were smaller in size (Figure S1E), in
154 agreement with the reduced developmental potential of IκBα-depleted mESCs [34].

155 To further study the requirement of IκBα in pluripotency exit *in vivo*, we established
156 teratomas by subcutaneous injection of IκBα-WT and IκBα-KO mESCs (Figure 2F and materials
157 and methods) into NSG (NOD.Cg-Prkdc^{scid} Il2rg^{tm1Wjl}/SzJ) mice. IκBα-KO teratomas showed a
158 decreased differentiation potential, as indicated by higher number of OCT4^{+} cells 6 weeks
159 after injection (Figures 2G-H). These observations further confirm the essential role of IκBα in
160 the exit from the pluripotency state not only *in vitro* but also under *in vivo* differentiation
161 signals. To understand the conditions in which IκBα is required for pluripotency exit, we
162 differentiated IκBα-WT and IκBα-KO mESCs cultured in Serum/LIF (naïve pluripotency)
163 towards EpiSCs (primed pluripotency) (Figure 3A, upper panel). IκBα-KO cells were not
164 committed towards the primed pluripotency stage and maintained an elevated expression
165 levels of naïve pluripotency genes (*Dppa3, Nanog, Sox2, Rex1, Klf2, Klf4, Gbx2, Tbx3*) (Figure
166 3A, bottom panel). Additionally, IκBα-KO cells retained a naïve pluripotent morphology,
167 forming tight clusters that resemble cells cultured in 2i/LIF medium (Figure S2A).

168 mESCs cultured in serum/LIF are highly heterogeneous, comprising a mixture of cell states
169 that resemble developmental transitions from preimplantation (naïve pluripotency) to
170 postimplantation (primed pluripotency) embryo [2,3]. To investigate how IκBα deficiency was
171 affecting the exit of mESCs from naïve pluripotency, we performed a Gene Set Enrichment
172 Analysis (GSEA) using RNA-seq data from IκBα-KO and IκBα-WT mESCs cultured in Serum/LIF

173 against gene signatures for 2i/LIF and Serum/LIF pluripotency [35]. GSEA results revealed a
174 significant enrichment in Serum/LIF IκBα-KO mESCs transcriptome for genes specifically
175 expressed in the naïve ground state (2i/LIF), while they negatively correlate with mESCs
176 cultured in Serum/LIF (Figure 3B) [35]. These results agree with the fact that IκBα-KO mESCs
177 cultured in Serum/LIF resemble 2i/LIF morphology, with homogeneous tight clusters of cells,
178 whereas IκBα-WT mESCs retain the colony heterogeneity (Figure S2B). Interestingly, the
179 higher levels of ground-state-related genes *Zfp42* (*Rex1*), *Klf2* and *Tbx3* in IκBα-KO mESCs
180 were partially obtained when IκBα-WT mESCs were cultured in 2i/LIF for two consecutive
181 passages (Figure 3C).

182 One of the key features of the naïve pluripotency state is its global DNA hypomethylation
183 pattern [15,16]. We assessed the DNA methylation status of IκBα-WT and IκBα-KO mESCs
184 cultured in Serum/LIF conditions by analysis of 5-methyl-cytosine (5mC) mark and using DNA
185 methylation arrays [36]. We found that IκBα-KO mESCs contained much lower levels of 5mC
186 compared to IκBα-WT cells (Figure 3D). Moreover, DNA methylation arrays confirmed a global
187 pattern of DNA hypomethylation in IκBα-KO mESCs, which was maintained in 96h EBs (Figure
188 3E). Interestingly, the DNA hypomethylation status occurred in a genome-wide fashion
189 affecting all chromosomes (Figure S2C), in accordance with a higher pluripotent state of IκBα-
190 KO mESCs.

191 Overall, these data demonstrate that IκBα is required for the exit of the naïve state of
192 pluripotency and its deficiency results in impaired differentiation of mESCs *in vivo* and *in vitro*.
193 Accordingly, IκBα-KO mESCs cultured in Serum/LIF showed genome-wide pattern of DNA
194 hypomethylation.

195 **Lack of IκBα causes an epigenetic rewiring in pluripotent stem cells to resemble 2i/LIF naïve**
196 **pluripotency in Serum/LIF culture**

197 ChIP Enrichment Analysis (ChEA) of genes identified in our RNA-seq data of IκBα-KO and WT
198 mESCs revealed that differentially expressed genes were putative targets of chromatin
199 regulators including the PRC2 subunit SUZ12 and MTF2 (Figure 4A). We previously described
200 that IκBα is important for the proper deposition of the H3K27me3 mark in different types of
201 tissue stem cells by associating with elements of the PRC2 complex [27,28]. Since 2i/LIF and
202 Serum/LIF states are characterized by important differences in epigenetic marks, we carried
203 out an epigenetic profiling of IκBα-WT and IκBα-KO mESCs cultured in Serum/LIF. We
204 performed chromatin immunoprecipitation followed by sequencing (ChIP-seq) of histone
205 modifications associated with gene activation (H3K4me3) and gene repression (H3K27me3)
206 (Figures 4B and S3A-B). Overall, Serum/LIF IκBα-KO mESCs exhibited a general increased
207 H3K4me3 status and redistribution of the PRC2-catalyzed H3K27me3 mark (Figure 4B).
208 Notably, gain of the H3K4me3 mark was associated with a reduction of H3K27me3 levels in
209 genes associated with naïve pluripotency function (Figures 4B-C and S3A-B). In particular, 41
210 genes with concomitant gain of H3K4me3 and loss of H3K27me3 were found to be enriched

211 in mechanisms associated with pluripotency function (Figure 4C), including Tbx3 and Gbx2
212 (Figure 4D-4E). A second set of pluripotency-related genes showed an increase in H3K4me3
213 without changes in H3K27me3 (Zfp42 or Klf2). Both sets of pluripotency genes showed
214 increased expression in the absence of IκBα (Figure 4H).

215 We next aimed to study whether the lack of IκBα was also affecting distal regulatory regions
216 by analyzing enhancer-associated histone marks in IκBα-WT and IκBα-KO mESCs. We
217 quantified the total amount of H3K27Ac (active enhancer) and H3K4me1 (poised enhancer)
218 by ChIP-seq experiments conducted in both IκBα-WT and IκBα-KO mESCs. Overall, IκBα-KO
219 mESCs showed a reduction in poised enhancers at genes (or related genomic regions)
220 associated with differentiation processes (Figures 4F and S3C) and an increase in active
221 enhancers at genes associated with pluripotency (Figure 4F and S3D), such as Tbx3, Tfcp2l1
222 and Zfp42 (Rex1) (Figure 4G), which positively favors their higher expression in IκBα-KO mESCs
223 (Figure 4H). These results further support that mESCs lacking IκBα are epigenetically
224 remodeled to favor the ground state of naive pluripotency, which may negatively impact on
225 their differentiation potential, similar to that described for other models with stabilized naïve
226 pluripotent state[37,38].

227 **The chromatin function of IκBα in pluripotency exit is independent of classical NF-κB**
228 **activity.**

229 Although previous results from C. elegans [39] and Drosophila [27] support the functional
230 relevance of chromatin-related IκBα function, the investigation of this alternative IκBα
231 activity remains challenging due to the predominant role of this protein in NF-κB regulation.
232 However, and similar to that found in other models, we did not detect major changes in
233 canonical NF-κB target genes upon IκBα depletion neither in Serum/LIF mESCs, nor 48h and
234 96h EB-differentiating conditions (Figure 5A). Thus, either NF-κB regulation does not require
235 IκBα at this stage or it might be compensated by the other IκBs (IκBβ, IκBε or p100), as
236 previously demonstrated [40,41].

237 To further investigate the relative impact of both IκBα functions in mESCs, we took advantage
238 of recent results from our group that led to the identification of the specific IκBα protein
239 residues that define NF-κB- or chromatin-binding through H2A/H4. Mutation of these
240 residues allowed the generation of doxycycline-inducible (i) separation-of-function IκBα
241 mutants that are specifically deficient in one or the other function, at least in the intestinal
242 epithelial cells[32]. We called i-IκBα$^{\Delta Chromatin}$ the i-SOF IκBα mutant that interacts with NF-κB
243 but is deficient for H2A and H4 binding and i-IκBα$^{\Delta NF\text{-}\kappa B}$ the one that interact with histones but
244 is deficient for NF-κB subunits binding (Figure 5B and [32]). The three different IκBα forms (i-
245 IκBα^{WT}, i-IκBα$^{\Delta NF\text{-}\kappa B}$ and i-IκBα$^{\Delta Chromatin}$) were stably transfected in the IκBα KO mESCs and
246 induced by 16h of doxycycline treatment (Figure S4A). We used these cells to investigate the
247 biochemical properties and functional impact of SOF IκBα mutants in mESCs. By pull-down
248 experiments, we found that i-IκBα$^{\Delta NF\text{-}\kappa B}$ expressed in ESCs was able to interact with histone

249 H2A but not with the NF-κB member p50. In contrast, i-IκBα$^{\Delta Chromatin}$ interacts with p50 but
250 not with H2A, while i-IκBα^{WT} preserves both binding capacities (Figure 5C). In concordance
251 with these results, i-IκBα^{WT} and i-IκBα$^{\Delta NF\text{-}\kappa B}$ were found in both the cytoplasmic and chromatin
252 fractions of mESCs, whereas IκBα$^{\Delta Cromatin}$ was retained in the cytoplasm (Figures 5D-E). In
253 multiple experiments, we noticed a significant reduction in protein levels of IκBα$^{\Delta chromatin}$
254 despite the mRNA expression levels of the different IκBα forms being comparable (Figures 5C-
255 D and S4A).

256 Then, we studied whether i-IκBα^{WT} and/or the i-SOF IκBα mutants (IκBα$^{\Delta NF\text{-}\kappa B}$ or IκBα$^{\Delta Chromatin}$)
257 were able to reverse any of the phenotypes observed in the IκBα-KO mESCs (Figure S4B).
258 Induction of i-IκBα^{WT} and i-IκBα$^{\Delta NF\text{-}\kappa B}$ reduced the expression levels of the naïve pluripotent
259 genes *Zfp42, Klf2, Sox2* and *Tbx3*. On the other hand, the same genes either do not change
260 their expression (*Zfp42, Sox2, Klf2*) or increase their levels (*Tbx3*) upon i-IκBα$^{\Delta Chromatin}$
261 induction (Figure 5F). In addition, the ground state-associated DNA hypomethylation was
262 specifically reverted in i-IκBα^{WT} and i-IκBα$^{\Delta NF\text{-}\kappa B}$ mESCs but not in i-IκBα$^{\Delta Chromatin}$ mESCs (Figure
263 5G). Finally, we addressed whether i-IκBα^{WT}, i-IκBα$^{\Delta NF\text{-}\kappa B}$ and i-IκBα$^{\Delta Chromatin}$ mESCs were
264 capable to revert the differentiation blockage of IκBα-KO ESCs (Figure S4B). Induction of
265 IκBα^{WT} and IκBα$^{\Delta NF\text{-}\kappa B}$ was enough to restore the differentiation potential of IκBα-KO mESCs
266 into EBs, as indicated the increase in the number of differentiated cells (based on percentage
267 of SSEA-1^{neg} cells) (Figures 5H and S4C) and the reduced number of AP+ colonies (in the 216h
268 IκBα-KO reconstituted EB assays), which was similar to the number of colonies obtained from
269 IκBαWT EBs (Figures 5I). Lastly, the number of remaining pluripotent-like cells (defined by
270 OCT3/4 NANOG staining) was also reduced in i-IκBα^{WT} and i-IκBα$^{\Delta NF\text{-}\kappa B}$ 216h EBs, and only
271 small and few regions of undifferentiated cells was observed. In contrast, induction of i-
272 IκBα$^{\Delta Chromatin}$ did not restore the differentiation potential of IκBα-KO mESCs (Figures 5J and
273 S4D).

274 These results demonstrate that the chromatin-dependent IκBα function, but not its NF-κB-
275 related activity, is necessary for the proper regulation of chromatin marks at specific genomic
276 regions that are linked to transcriptional changes that are likely at the base of the capacity of
277 ESCs to exit the ground state of naïve pluripotency and differentiate.

278 **DISCUSSION**

279 Here we have identified a new and unexpected function for the IκBα protein in the regulation
280 of the naïve pluripotency exit. Using mESCs to investigate the role of IκBα in pluripotency
281 maintenance and differentiation, we discovered that the absence of IκBα severely impairs the
282 exit of pluripotency. Furthermore, IκBα-KO mESCs stabilizes the ground state of naïve
283 pluripotency under Serum/LIF conditions, shedding light on its function as a critical regulator
284 of the transition from naïve to primed pluripotency. While IκBα is commonly known for its
285 role as an inhibitor of the NF-κB signaling pathway [26], our laboratory has previously furnished
286 compelling evidence of its alternative role through its interaction with histones and other
287 chromatin components [27,29,31]. We have demonstrated that chromatin-bound IκBα plays a
288 crucial role in regulating skin and intestinal stem cells [27,28], hematopoietic stem cell
289 development [42], and it influences the regenerative capacity of these tissues, and in some
290 cases, their susceptibility to neoplastic transformation. Disentangling the chromatin-related
291 function of IκBα from its canonical role as an inhibitor of NF-κB has been challenging, making
292 it difficult to determine its truly biological significance. To tackle this challenge, we engineered
293 separation-of-function (SOF) mutants of IκBα, as detailed in [43], by identifying specific residues
294 that are essential for binding either NF-κB elements or histones. Interestingly, we have shown
295 that only the histone-binding proficient IκBα mutant (IκBα$^{\Delta NF\text{-}\kappa B}$), which lacks the ability to
296 bind to NF-κB, has the capability to reverse the stabilization of the ground state observed in
297 IκBα-KO mESCs. This is sufficient to facilitate their exit from the state of naïve pluripotency,
298 restoring their full differentiation potential (Figure 5). The involvement of NF-κB in
299 pluripotency has been a subject of prior investigation. Studies have revealed that pluripotent
300 cells display a dampened inflammatory signaling pathway, which is induced upon
301 pluripotency dissolution and activation of differentiation [24,44]. However, the precise molecular
302 mechanisms underlying the attenuated status of NF-κB during this stage remain incompletely
303 understood. A recent work has shed light on a potential regulatory axis involving ATG5-β-
304 TrCP1-NF-κB, proposing it as a mechanism that diminishes NF-κB activity by stabilizing the
305 IκBα protein in mESCs [23]. In any case, since modification of canonical NF-κB activity directly
306 impacts on the levels IκBα expression, the previous NF-κB-associated phenotypes should be
307 reevaluated considering this chromatin role of IκBα. Furthermore, the expression of
308 IκBα$^{\Delta Chromatin}$, which retains the inhibitory function of NF-κB, failed to mitigate the ground
309 state stabilization observed in IκBα-KO mESCs (Figure 5). This finding suggests that the
310 observed role of IκBα in regulating the exit from naïve pluripotency is not due to NF-κB
311 inhibition. In fact, there is evidence that the chromatin function of IκBα is an ancestral
312 function preceding its role as NF-κB inhibitor. In Caenorhabditis Elegans (*C.elegans*), which
313 lacks NF-κB orthologs but possesses two homologs of IκBα, the absence of IκBα orthologs has
314 severe multi-organ differentiation defects [39]. This observation further supports the notion
315 that the chromatin-related function of IκBα plays a fundamental role in developmental
316 processes, independent of its canonical role in NF-κB signaling. Nonetheless, differences in

317 the expression level of SOF IκBα mutants, with the IκBα$^{\Delta Chromatin}$ expressed at lower protein
318 levels compared to the IκBα$^{\Delta NF\text{-}\kappa B}$, may also impact in the rescue phenotype.

319 We have observed that IκBα-KO mESCs exhibit epigenetic and transcriptomic profiles
320 resembling the ground state of naïve pluripotency under Serum/LIF culture (Figure 3). In this
321 regard, the fact that IκBα is preferentially located in the chromatin of mESCs cultured in
322 Serum/LIF, when they exhibit a high degree of heterogeneity, suggests that IκBα might act as
323 a regulator of this heterogeneity. One potential explanation might be that IκBα could be
324 affecting the stability of fluctuating transcription factors, which is crucial to mediate the
325 pluripotent-to-differentiation balance [3]. Thus, the lack of IκBα might stabilize those
326 transcription factors that would favor the ground-state observed in IκBα-KO mESCs cultured
327 in Serum/LIF. Although IκBα KO mESCs exhibit a transcriptional phenotype and
328 hypomethylation state that resembles the ground state of naïve pluripotency, there are only
329 modest changes on histone marks associated to enhancers (H3K27Ac) or gene regulation
330 (H3K4me3 and H3K27me3). Altogether indicates that further experiments are required to
331 fully elucidate the effect of chromatin IκBα. Moreover, the differences in murine and human
332 pluripotency [11] point out the necessity to address the real impact of IκBα modulation in the
333 stabilization of the ground state in human pluripotent stem cells.

334 In summary, our work establishes that IκBα mediates the exit from naïve pluripotency by
335 modulating the activation of naïve pluripotency genes. Importantly, this newly identified role
336 of IκBα operates independently of its canonical function in inhibiting the NF-κB pathway. Our
337 findings underscore the intricate interplay between inflammation and pluripotency status,
338 revealing a previously unrecognized complexity in their interaction.

339 **METHODS**

340 **Cell culture**

341 mESC line ES-E14TG2a (ATCC; Cat #CRL-1821) was cultured on plastic dishes precoated with
342 0.1% (w/v) Gelatin (Sigma; Cat #G2500-100G) in Serum/LIF medium. Serum/LIF is composed
343 by DMEM basal medium (Sigma-Aldrich; Cat #D5796) supplemented with 15% FBS (ESC-
344 qualified; Gibco Cat #26140079), 1X Glutamax (Gibco; Cat #35050061), 1X NEAA (Gibco;
345 Cat#11140050), 1mM Sodium Pyruvate (Gibco; Cat#11360070), 1000U/mL Leukemia
346 Inhibitory Factor (LIF) (Millipore, Cat #ESG1107) and 0.125mM 2-mercaptoethanol (Gibco;
347 Cat#31350010). Medium was changed every day, and cells were splitted every other day using
348 TrypLE Express (Gibco; Cat #12605010) for harvesting. Cells were maintained in a 5% CO2
349 incubator at 37°C.

350 For inducing the ground-state of naïve pluripotency, mESCs were cultured in 2i/LIF medium
351 for 2 consecutive passages. 2i/LIF medium is composed by NDiff 227 medium (TAKARA, Cat
352 #Y40002) supplemented with 1000U/mL LIF, 0.4 µM PD032591 (Selleck Chemicals, Cat
353 #S1036) and 3 µM CHIR99021 (Merck, Cat #SML1046).

354 **Epiblast stem cell differentiation**

355 Differentiation from mESCs towards Epiblast Stem Cells (EpiSCs) was performed as previously
356 described [45]. $3x10^4$ mESCs were seeded in 6-well plastic dishes, and they were cultured in
357 Serum/LIF medium for 24h. Medium was then switched to NDiff 227 medium (TAKARA, Cat
358 #Y40002) supplemented with 20 ng/ml activin A (Cat. #120-14E; PeproTech) and 10 ng/ml Fgf
359 basic (R&D Systems, Cat #233-FB-025/CF). Cells were submitted to daily media changes till
360 day 5 (120h), when they were further analyzed.

361 **Embryoid bodies differentiation from mESCs**

362 Embryoid bodies differentiation was established as described in [46]. Briefly, mESCs were
363 splitted twice in Serum/LIF medium before inducing differentiation. Once mESCs are 80%
364 confluent, cells were collected using TrypLE Express. One well of 6-well plate was splitted in
365 an entire 6-well plate in IMDM-ES medium for 48h. IMDM-ES medium is composed of Iscove's
366 Modified Dulbecco's Medium (IMDM) (Cytiva, Cat #16SH30259.01) supplemented with 20%
367 FBS (ESC-qualified; Gibco Cat #26140079), 1X Glutamax (Gibco; Cat #35050061), 1X NEAA
368 (Gibco; Cat#11140050), 1mM Sodium Pyruvate (Gibco; Cat#11360070), 10ng/mL Leukemia
369 Inhibitory Factor (LIF) (Millipore, Cat #ESG1107) and 0.125mM 2-mercaptoethanol (Gibco;
370 Cat#31350010). For embryoid body induction, mESCs were harvested, and they were rinsed
371 twice with DPBS (Gibco; Cat #14190144). Cells were very well disaggregated into single-cells,
372 and 1.2 x 10^4 cells/mL embryoid body differentiation (EB^{diff}) medium were resuspended to a
373 total volume of 25mL of EB^{diff} medium. EB^{diff} medium is composed by IMDM supplemented
374 with 15% FBS (ESC-qualified; Gibco Cat #26140079), 1X Glutamax (Gibco; Cat #35050061), 50

375 µg/mL ascorbic acid (Sigma; Cat #A-4544), 180 µg/mL Transferrin (Roche; Cat #10652202001)
376 and 0.45 mM alpha-monothioglycerol (MTG) (Sigma; Cat #M6145). EBs were formed in
377 suspension for 5 days (120h). At day 5, in order to elongate the differentiation up to 216h
378 (day 9), EB^{diff} medium was refreshed by harvesting EBs with 10mL serological pipette,
379 centrifuge at 200 g for 3 min and EBs were resuspended in fresh EB^{diff} medium for 4 more
380 days.

381 **CRISPR/Cas9 gene editing and cell lines generation in mESCs**

382 The two guide RNAs (gRNAs) targeting the Nfkbia locus were designed using the CRISPR design
383 tool from MIT (http://crispr.mit.edu). The best 2 gRNAs (based on on-target and off-target
384 scores) that were targeting the exon 1 of Nfkbia (IκBα gene) were selected. After annealing,
385 one of the gRNAs was cloned into SpCas9(BB)-2A-GFP (px458) plasmid (Addgene; Cat #48138),
386 and the other gRNA was cloned into the px330-mCherry plasmid (modified from Addgene;
387 Cat #98750 to incorporate mCherry reporter). mESCs were co-transfected with the two
388 plasmids (px458-gRNA1 and px330-mCherry-gRNA2). $3x10^5$ cells were seeded a day before
389 per well of 6-well plate. At day of transfection, cells were washed once with 1X DPBS (Gibco;
390 Cat #14190144), and 2mL Opti-MEM medium (Gibco; Cat #31985070) was added into cells.
391 1.25 µg of each plasmid (2.5 µg of total DNA) was incubated with 10 µL of Lipofectamine 2000
392 (Invitrogen; Cat #11668019) in 240 µL of Opti-MEM for 20 min.
393 OptiMEM::Lipofectamine::DNA mixture was added into mESCs, and cells were incubated for
394 5 hours. Cells were then washed with DPBS, and medium was replaced by Serum/LIF. 48h
395 after transfection, GFP^+ $mCherry^+$ single cells were sorted by FACS using BD FACSAria II Cell
396 Sorter (BD Bioscience). Mutant clones were screened through PCR and western blotting to
397 identify single clones with no IκBα protein expression. Non-targeting scrambled gRNAs were
398 cloned into px458 and px330-mCherry plasmids as wildtype clones. Three independent clones
399 from each genotype (IκBα-WT and IκBα-KO) were selected for further experiments.

400 Doxycycline-inducible IκBα ($IκBα^{WT}$, $IκBα^{ΔNF-κB}$ and i-$IκBα^{ΔH2A/H4}$) mESCs were generated by
401 cloning the three different IκBα versions into a PiggyBac transposon system [47]. IκBα protein-
402 coding cDNAs were PCR-amplified, and NheI and SalI restriction sites were placed at the 5'
403 and 3' ends, respectively. T2A-EGFP fragment was amplified from PX458 plasmid, and SalI and
404 AgeI restriction sites were introduced at its 5' and 3' ends. PB-TRE backbone (Addgene, Cat#
405 63800) was digested with NheI and AgeI enzymes, and mNfkbia and T2A-EGFP fragments
406 were ligated into the PB-TRE digested vector. To generate mESCs containing the inducible
407 vector, IκBα-KO mESCs were co-transfected with PB-TRE-mNfkbia-T2A-EGFP and PiggyBac
408 transposase plasmids, and pool of transfected cells was selected by Hygromycin (100µg/mL)
409 for 7 days. Cells were doubly screened by FACS sorting green fluorescent protein after 24h of
410 doxycycline (1µg/mL) treatment. Pool of cells were used for further experiments. Oligos
411 sequences are included in supplementary table 1.

412 **Teratoma formation assay**

413 IκBα-WT and IκBα-KO mESCs grown in Serum/LIF (5×10^5) were injected intramuscularly into
414 severe combined immunodeficient mice (NSG). In order to favor 3D aggregation of cells and
415 teratoma formation, cells were resuspended in Matrigel Matrix (BD; Cat #356234) prior to
416 injection. Six weeks later, mice with tumors were euthanized, and tumors were fixed in
417 formaldehyde, embedded in paraffin, sectioned and stained with hematoxylin and eosin for
418 histological analysis.

419 **Immunofluorescence staining**

420 For immunostaining of mESCs, cells were seeded on 0.1% gelatin-coated coverslips on 6-well
421 plates; for EB immunofluorescence, they were collected directly from the plate. Samples were
422 washed twice with 1X PBS, and they were fixed at 4ºC for 30 minutes with 4% PFA (Electron
423 Microscopy Sciences; Cat #15713S). For immunofluorescence of 5-Methylcytosine (5mC),
424 fixed cells were incubated with 2M Hydrochloric Acid (Sigma-Aldrich, Cat #H1758) for 20
425 minutes at room temperature. Samples were then washed twice with 1X Tris-buffered saline
426 (TBS; 50 mM Tris-Cl, pH 8) and permeabilized and blocked with 1X TBS supplemented with 1%
427 Triton-X100 (MERCK; Cat #9036-19-5) and 6% FBS (Biological Industries; Cat #04-001-1A) for
428 2h at 4ºC. Samples were washed twice with 1X TBS supplemented with 6% FBS. Primary
429 antibody incubation was performed in 1X TBS plus 6% FBS and 0.3% or 0.5% Triton-X100 (0.3%
430 for 2D culture and 0.5% for EBs) overnight at 4ºC. The following primary antibodies were used:
431 OCT3/4 (1:250; Santa Cruz; Cat #sc-5279), NANOG (1:250; Novus Biologicals; Cat #NB100-
432 588), 5-Methylcytosine (1:500, Invitrogen, Cat #MA5-24694), H3K27Ac (1:2000, Abcam, Cat
433 #AB4729). Samples were then washed 4 times with 1X TBS, 5 min each washing. Secondary
434 antibody incubation was performed in TBS 1X plus 1% BSA (Sigma-Aldrich; Cat #9048-46-8)
435 for 2h at room temperature. The following antibodies were used: Alexa Fluor 488 donkey anti-
436 mouse antibody (1:1000; Invitrogen; Cat #A-21202), Alexa Fluor 647 donkey anti-mouse
437 antibody (1:1000; Invitrogen; Cat #A-31571), Alexa Fluor 594 donkey anti-rabbit antibody
438 (1:1000; Life Technologies; Cat #A-21207), Alexa Fluor 647 donkey anti-rabbit
439 antibody(1:1000, Invitrogen; Cat #A-31573). Samples were washed three times with 1X TBS
440 for 5 min at room temperature each rinse. Samples were mounted using DAPI Fluoromount-
441 G (Southern Biotech; Cat #0100-20).

442 **Microscopy and image acquisition**

443 Fluorescence images were acquired using Confocal Leica TCS SP5 (Leica Microsystems), and
444 Leica application software LAS AF (Leica Microsystems) was used to visualize the images.
445 Images of teratoma haematoxylin and eosin and immunohistochemistry stainings were
446 acquired using BX61 Olympus Microscope (Olympus), and PRECiV™ 2D Image and
447 Measurement Software (Olympus) was used to visualize the images. The Image J (version
448 1.15) was used for further analysis [48].

449 **Flow cytometry sample preparation and analysis**

450 Cells were collected and they were purified based on FACS using BD FACSAria II Cell Sorter
451 (BD Bioscience). Cells were sorted at 3,500 events/second, and at maximum flow rate of 4
452 and 85 µm nozzle. 5 µg/ml of DAPI (Biotium; Cat #BT-40043) was used as a viability dye. For
453 flow cytometry analysis of pluripotency exit, cells were disaggregated using TrypLE Express,
454 and they were incubated at 4ºC for 20 minutes with SSEA1-eFluor 660 Monoclonal Antibody
455 (1:200, Invitrogene, Cat #50-8813-42). BD LSRFortessa Cell Analyzer or BD LSR II Flow
456 Cytometer (BD Bioscience) were used for Flow Cytometry Analysis experiments. Flow
457 cytometry data were analyzed using FlowJo X v10.0.7 (BD Biosciences).

458 **RNA isolation, cDNA synthesis and quantitative RT-PCR**

459 Total RNA isolation from cells was performed using the RNeasy Plus Mini Kit (Qiagen; Cat
460 #74136) or RNeasy Micro Kit (Qiagen; Cat #74004) following manufacturer's instructions.
461 Amount of RNA was quantified with Nanodrop (Thermo Fisher; Cat #ND2000CLAPTOP), and
462 2 µg of total RNA was retro-transcribed using Transcriptor First Strand cDNA Synthesis Kit
463 (Roche; Cat #04897030001) following the manufacturer's instructions.

464 Quantitative RT-PCR was performed in triplicates for each sample, and SYBR Green I Master
465 Kit (Roche; Cat #04887352001) was used to carry out the reaction. qRT-PCR was performed
466 using the LightCycler 480 system (Roche). Relative expression levels were calculated as $2^{-\Delta CT}$
467 normalized with the average CT of the housekeeping gene Tbp or Gapdh. Oligos sequences
468 are found in supplementary table 1.

469 **Chromatin Immunoprecipitation (ChIP)**

470 4-6x10^7 mESCs were cross-linked by incubating them in DPBS (Gibco, Cat #14190094)
471 supplemented with 1% formaldehyde (Sigma-Aldrich; Cat #252549) for 10 min rocking at
472 room temperature. Cross-linking was stopped using 125 mM Glycine (Sigma-Aldrich, Cat
473 #G8790) rocking for 5 minutes at room temperature. Fixed cells were then washed twice with
474 ice-cold DPBS, and scrapped and collected using DPBS supplemented with
475 protease/phosphatase inhibitor cocktail composed by 1X cOmplete™, EDTA-free Protease
476 Inhibitor Cocktail (Roche, Cat #11873580001), 1 mM PMSF, 1mM Sodium Ortovanadate and
477 20 mM β-Glycerol phosphate. Cells were centrifuged at 3200g for 5 minutes at 4ºC. Cells were
478 lysed by resuspending cell pellet in ice-cold ChIP buffer (1 volume of SDS buffer [100mM NaCl,
479 50mM Tris-HCl pH 8.1, 5mM EDTA pH 8, 0.5% SDS] and 0.5 volume of triton dilution buffer
480 [100mM Tris-HCl pH 8.6, 100mM NaCl, 5mM EDTA pH 8, 5% Triton X-100]) supplemented with
481 protease/phosphatase inhibitor cocktail, and samples were sonicated using sonication beads
482 (Diagenode; Cat #C01020031) and the Bioruptor Pico Sonicator (Diagenode; Cat #B01060010)
483 for 20 cycles (each cycle 30 seconds on/30 seconds off) or till DNA fragments have 100-300bp
484 size. Samples were centrifuged at 16000g for 20 minutes at 4ºC. Chromatin was quantified,
485 and 30 µg of chromatin was incubated with every 5µg of antibody rotating for 16 hours (or
486 overnight) at 4ºC. The following antibodies were used: H3K4me3 (Abcam, Cat #ab8580),

487 H3K27me3 (Millipore, Cat ##07-449), H3K27Ac (Abcam, Cat #ab4729), H3K4me1 (Abcam, Cat
488 #ab8895). Samples were pulled down by incubation with Protein A-Sepharose™ CL-4B
489 (previously hydrated and blocked with 0.05% BSA) for 3h at 4ºC in rotation. Sample was
490 washed with a low salt washing buffer (50mM HEPES pH 7.5, 140mM NaCl and 1% Triton)
491 three times, one wash with a high salt wash buffer (50mM HEPES pH 7.5, 500mM NaCl and
492 1% Triton) and one wash with TE pH 8 (10mM Tris-HCl pH8, 1mM EDTA). Samples were then
493 eluted in 1% SDS and 100mM $NaHCO_3$. Samples were descrosslinked by incubating for 16
494 hours (or overnight) at 65ºC shaking at 450 rpm, and were treated with Proteinase K for 1h at
495 45ºC. DNA was purified using QIAquick PCR Purification Kit (Qiagen, Cat #28106), following
496 the manufacturer's instructions.

497 For ChIP followed by sequencing (ChIP-seq) Purified DNA concentration and integrity were
498 determined using Agilent Bioanalyzer (Agilent Technologies; Cat #G2939BA). Libraries were
499 prepared using standard protocols. Chromatin was sequenced using Illumina HiSeq platform
500 (Illumina, Inc.) (50bp single-end reads). Samples sequencing depth range was the following:
501 (i) H3K4me3: 2.56-2.74x10^7 reads, (ii) H3K27me3: 6.19-7.2x10^7 reads, (iii) H3K27Ac: 9.11-
502 10.65x10^7 reads and (iv) H3K4me1: 9.76-10.58x10^7 reads.

503 **ChIP-seq data analysis**

504 Quality control was performed on raw data with FASTQC tool. Raw reads were trimmed to
505 remove adapters presence with Trimgalore (v0.6.6) [49]. Default parameters were used except
506 for a minimum quality of 15 (Phred score) and an adapter removal stringency of 3bp overlap.
507 For H3K4me3, H3K27me3 and H3K4me1 data, trimmed reads were aligned to the reference
508 genome with Bowtie2 (v2.4.4) which was executed with default parameters [50]. Required
509 genome index was built with corresponding GRCm38 fasta file retrieved from Ensembl
510 (http://ftp.ensembl.org/pub/release-102/). Multimapped reads and those exhibiting MAPQ <
511 20 were removed. Randomly placed multi mappers were removed from the mapped reads.
512 For all cases, duplicated reads were marked with SAMtools (v1.15) [51]. Drosophila
513 Melanogaster spike-ins, present in H3K27me3, were discarded. NSC and RSC quality metrics
514 were computed with PhantomPeakQualTools (v1.2) [52]. ENCODE blacklisted regions (mm10
515 v2) were removed prior to peak calling. BigWig files were individually generated using
516 deepTools (v3.5.1) bamCoverage with -ignoreDuplicates -binSize 10 -smoothLength 30 -
517 effectiveGenomeSize 2308125349 -normalizeUsing RPGC and -extendReads
518 *Fragment_Length* options [53]. The effective genome size was particularized to a read length of
519 50bp and directly retrieved from deepTools web site
520 (https://deeptools.readthedocs.io/en/develop/content/feature/effectiveGenomeSize.html).
521 *Fragment_Length* was retrieved from PhantomPeakQualTools results. For all histone marks
522 except for H3K4me3, peak calling was conducted by means of epic2 (v0.0.52) with -effective-
523 genome-fraction 0.8452 -fragment-size *Fragment_Length* options and chromosome sizes
524 only referring to canonical chromosomes [54]. For H3K4me3, MACS2 (v2.2.7.1) was used to
525 identify peaks with -nomodel -extsize *Fragment_Length* -g 2308125349 options [55]. The

526 corresponding input sample was used in all peak calling computations. For the histone marks,
527 peaks were called with adjusted p-values (FDR) < 0.05.

528 Peak annotation was performed with ChIPseeker R (v4.2.1) package (v1.34.1) considering a
529 TSS region range between 5000 bp upstream and 100 bp downstream (Yu et al., 2015).
530 Required TxDb object was generated from the Ensembl GRCm38 gtf file retrieved
531 (http://ftp.ensembl.org/pub/release-102/). A consensus peakset was obtained from the
532 three biological replicates per histone mark and condition (IκBα-WT or IκBα-KO) by identifying
533 overlapping peaks in at least two out of the three replicates.

534 Differential binding analysis (DBA) was conducted with DiffBind (v3.8.4) per histone mark [56].
535 Default parameters were used except for the summits parameter which was set to 500bp for
536 all histone marks except for H3K4me3 (150bp) in order to consider, for testing, intervals of
537 1000bp or 300bp respectively. Summit values were selected to have interval widths between
538 the minimum and first quartile peak width values for each histone mark. EdgeR was the
539 statistical method used for all the three analyses. Differentially bound regions (DBRs)
540 between IκBα-KO and IκBα-WT samples were called with adjusted p-values (FDR) < 0.05.
541 Identified DBRs with any annotated gene were plotted with EnrichedHeatmap R package
542 (v1.18.1) [57]. To summarize replicates per condition, normalizeToMatrix function was used
543 based on corresponding BigWig files in w0 mean mode in 50bp windows. Tracks visualization
544 were obtained by means of Integrative Genomics Browser (IGV) tool [58]. List of DBA regions
545 are listed in supplementary table 2.

546 **Enhancers activity identification**

547 Consensus peaksets derived from the three H3K27ac and H3K4me1 IκBα-WT mESCs replicates
548 were used to identify poised and active enhancers in an IκBα-WT scenario. Putative poised
549 enhancers were defined as those regions with H3K4me1 but no H3K27ac peaks. Putative
550 active enhancers were defined as those regions with H3K27ac and presence/absence
551 H3K4me1 peaks. To assess any differential enhancers activity in IκBα-KO vs IκBα-WT mESCs
552 cultured in Serum/LIF, differentially bound regions and consensus peaksets (IκBα-KO)
553 identified in H3K4me1 and H3K27ac were required. Putative gained or lost poised/active
554 enhancers in IκBα$^{-/-}$ were obtained with following criteria: (i) for gained/lost poised enhancers
555 in IκBα$^{-/-}$: a differential H3K4me1 increase/decrease and absence of H3K27ac peaks in IκBα$^{-/-}$
556 consensus peakset, (ii) for gained/lost active enhancers (without H3K4me1) in IκBα-KO: a
557 differential H3K27ac increase/decrease and absence of H3K4me1 in IκBα-KO consensus
558 peakset and (iii) for gained/lost active enhancers (with H3K4me1) in IκBα-KO: a differential
559 H3K27ac increase/decrease and presence of H3K4me1 in IκBα$^{-/-}$ consensus peakset. List of
560 differential enhancers are listed in supplementary table 2.

561 A maximum gap of 1000bp was allowed for checking the overlap between two different
562 histone marks. For this purpose, the 'subsetByOverlaps' function from the IRanges R package
563 was used (v.2.34.1).

564 **RNA-seq experiments**

565 Total RNA from three independent clones from mESCs, 48h EBs and 96h EBs was isolated
566 using the RNeasy Plus Mini Kit (Qiagen; Cat #74136) following manufacturer's instructions.
567 Amount of RNA was quantified with Nanodrop (Thermo Fisher; Cat #ND2000CLAPTOP), and
568 RNA integrity was addressed by agarose gel and Agilent Bioanalyzer (Agilent Technologies;
569 Cat #G2939BA). Libraries sequenced using Illumina HiSeq 2500 (Illumina, Inc.) (125bp paired-
570 end reads). Samples sequencing depth ranged between 35M and 52M reads (average 41M
571 reads) per sample.

572 **RNA-seq data analysis**

573 Quality control was performed on raw data with the FASTQC tool (v0.11.9). Raw reads were
574 trimmed to remove adapter presence with Trimgalore (v0.6.6) [49]. Default parameters were
575 used except for a minimum quality of 15 (Phred score) and an adapter removal stringency of
576 3bp overlap. Trimmed reads were aligned to reference the genome with STAR aligner tool
577 (v2.7.8). STAR was executed with default parameters except for the number of allowed
578 mismatches which was set to 1. Required genome index was built with corresponding
579 GRCm38 gtf and fasta files retrieved from Ensembl (http://ftp.ensembl.org/pub/release-
580 102/). Obtained BAM files with uniquely mapped reads were considered for further analysis.
581 Raw gene expression was quantified using featureCounts tool from subRead software (v2.0.1)
582 with exon as feature [59]. The raw counts matrix was imported into the R Statistical Software
583 environment (v4.2.1) for downstream analysis. Raw expression matrix included 55,487 genes
584 per 18 samples in total. Experimental design considered three timepoints: mouse ESCs, EBs
585 at 48h and EBs at 96h. Each time point included 6 samples distributed in two conditions: 3
586 IκBα-WT and 3 IκBα-KO. Prior to statistical analysis, those genes with less than 10 raw counts
587 across the 6 samples under test were removed. After pre-filtering, 21,843 genes (mESCs),
588 21,424 genes (EBs 48h) or 21,664 genes (EBs 96h) were available for testing. For visualization
589 purposes, counts were normalized by the variance-stabilizing transformation method as
590 implemented in DESeq2 R package [60] (v1.38.3). Differential expression analysis (DEA) was
591 conducted with DESeq2. Each time point was independently analyzed. Fitted statistical model
592 included sample conditions as covariable with IκBα-WT as the reference. Obtained log2 fold
593 change values were shrunken with apeglm shrinkage estimator R package (v1.20.0) [61]. Raw p-
594 values were adjusted for multiple testing using the Benjamini-Hochberg False Discovery Rate
595 (FDR) [62]. Differentially Expressed Genes (DEGs) between IκBα-KO and IκBα-WT samples were
596 called with adjusted p-values (FDR) < 0.05 and absolute shrunken log2 Fold change > 1. Data
597 visualization was performed with the ggplot2 (v3.4.1). List of differentially expressed genes
598 (DEGs) are found in supplementary table 3.

599 **Genome-wide DNA methylation samples preparation**

600 DNA from frozen mESCs pellets was extracted using DNeasy Blood and Tissue Kit (Qiagen
601 GmbH, Hilden, Germany). Purified genomic DNA was quantified with Qubit (Invitrogen,
602 Carlsbad, CA, USA) according to manufacturer's instructions. Infinium Mouse Methylation
603 BeadChip (Illumina, Inc., San Diego, CA, USA) arrays were used to profile DNA methylation
604 genome wide. This platform allows over 285,000 methylation sites per sample to be
605 interrogated at single-nucleotide resolution. The samples were bisulfite converted using EZ
606 DNA Methylation-Gold™ Kit (Zymo Research, CA, USA) and were hybridized in the array
607 following the manufacturer's instructions.

608 **DNA methylation data analysis**

609 The DNA methylation profile of the studied samples was assessed using the Infinium Mouse
610 Methylation BeadChip Array (~285,000 methylation sites) as previously described [63]. Briefly,
611 raw signal intensities were obtained with GenomeStudio Software 2011.1 (Illumina) and DNA
612 methylation beta values were computed from raw IDAT files using GenomeStudio default
613 normalization with control probes and background subtraction. Quality control steps to
614 remove erratic probe signals were performed within the R statistical environment (v4.0.3).
615 We removed probes with detection p value > 0.01, genotyping probes and manufacturing
616 flagged (MFG) probes described in the Illumina manifest file
617 (https://support.illumina.com/downloads/infinium-mouse-methylation-manifest-file.html).
618 The differentially methylated probes (DMPs) between IκBα-WT and IκBα-KO samples were
619 computed separately for each time point (mESCs and EBs at 96h) by deriving a linear model
620 with the limma R package (v3.46.0). Each condition included 3 samples per time point. DMPs
621 with adjusted p-value (FDR) <0.05 and absolute mean methylation beta value difference
622 between conditions >0.3 were considered significant. DNA methylation analysis was
623 performed using the mm10 mouse genome reference build and the complete annotation was
624 downloaded from the annotated manifest file
625 (http://zwdzwd.github.io/InfiniumAnnotation#mouse) [36]. List of differentially DNA
626 methylated regions are listed in supplementary table 4.

627 **Functional analysis**

628 Overrepresentation analysis was applied over lists of selected genes derived from RNA-seq
629 data (DEGs) or from ChIP-seq data (differentially bound regions). The Gene Ontology
630 (Biological Process ontology, GO BP terms), KEGG PATHWAY and WikiPathways databases for
631 Mus Musculus [64–66] were interrogated by means of clusterProfiler R package (v4.6.2) (Wu et
632 al., 2021). Corresponding Entrez identifiers were used. Benjamini-Hochberg procedure was
633 used to obtain adjusted p-values. Obtained GO BP terms were simplified using the simplify
634 function from clusterProfiler with default parameters. Overrepresented terms or processes
635 were called with adjusted p-values (FDR) < 0.05.

636 Gene Set Enrichment Analysis (GSEA) was performed for mESCs against naïve and ground
637 state pluripotency signatures defined by other authors [35.]. For this purpose, the complete
638 list of genes from mESCs samples (21,843 genes) was ranked based on the shrunken log2 Fold
639 Change obtained from DEA. GSEA was conducted through the fgseaMultilevel function from
640 fgsea R package (v1.24.0) [68] with default parameters except for maxSize = 600 and eps=0.
641 Enrichment plots were generated with the same package.

642 Additionally, the testEnrichment function from SeSAMe R package (v1.14.2) [69] was used for
643 conducting functional analysis with default parameters over the list of DMPs. Probe design,
644 transcription factor binding site and histone modifications consensus database sets, included
645 in the same package, were interrogated.

646 Gene Set Variation Analysis (GSVA) R package (v1.46.0) with default parameters were used to
647 obtain Z-score values for genes annotated to endoderm (GO:0001706), mesoderm
648 (GO:0001707) and ectoderm (GO:0001705) GO BP terms [70].

649 **Statistical analysis**

650 Statistical analysis was performed with GraphPad Prism v.8.0.1. (GraphPad Software, Inc.).
651 Unless specified, the comparison between two groups was performed with unpaired two-
652 sided t-test. A p-value < 0.05 was considered significant.

653 **DATA AVAILABILITY**

654 All sequencing data is deposited at GEO under a SuperSeries with the accession number
655 GSE239565)[https://www.ncbi.nlm.nih.gov/geo/query/acc.cgi?acc=GSE239565]. Individual
656 SubSeries can be found at: GSE239563 (RNA-seq data), GSE239564 (ChIP-seq data) and
657 GSE239562 (Methylation array data).

658 **CODE AVAILABILITY**

659 Scripts used to process the generated bulk RNA-seq and ChIP-seq data are available in Github
660 repository: https://github.com/BigaSpinosaLab/PAPER_IkBa_Naive_Pluripotency

661 **ACKNOWLEDGEMENTS**

662 We would like to acknowledge all members of the Bigas/Espinosa labs for helpful discussions.
663 We are grateful for technical support to CRG/UPF Flow Cytometry Unit, CRG Genomics and
664 Advanced Light Microscopy Units. This work has been supported by Spanish Ministry of
665 Science and Innovation (PID2019-104695RB-I00, PLEC2021-007518, PDC2021-120817-I00),
666 Generalitat de Catalunya (2021SGR 39) and Departament de Salut (SLT002/16/00299) to AB;
667 the Spanish Ministry of Science and Innovation (PID2019-108322GB-100 and PID2022-
668 142679NB-I00) to LDC; the Spanish Ministry of Science and Innovation (PID2021-123383NB-
669 I00.) and the Agencia de Gestió d'Ajuts Universitaris i de Recerca (2021 SGR 01222) to BP.
670 L.G.P has been a recipient of FI AGAUR fellowship (2019 FI-B 00151/2020 FI_B1 00130) from
671 Generalitat de Catalunya. D.A-V was funded by the FIS fellowship (FI20/00130) from Instituto
672 Carlos III. M.B. received funding from the Ramón Areces Foundation. M.M. is a recipient of a
673 grant from the Instituto Carlos III, grant number CA22/00011 (co-funded by the European
674 Social Fund Plus, ESF+ and by the European Union).

675

676

677 **AUTHOR CONTRIBUTION**

678 L.G.P, L.E and A.B designed the study. L.G.P, D.A-V, M.B, A.I, J.G, J.B, D.A.E, C.A.G.P, C.B, V.R.C
679 and A.V performed experiments. L.G.P, M.M, M.B and C.A.G.P performed bioinformatics
680 analysis. L.G and A.B wrote the manuscript with input from all authors. C.B, A.V, A.V, P.M,

L.D.C, G.S, B.P, M.E and L.E provided input on experimental design. L.E and A.B provided resources and supervised the research.

683 **FIGURE LEGENDS**

684 **Figure 1. IκBα is highly expressed in pluripotent cells. A.** Schematic of pluripotent states in
685 mouse embryonic stem cells (mESCs). mESCs were maintained regularly in naïve pluripotency
686 by culturing them in serum/LIF medium, or they were polarized towards the ground state of
687 naïve pluripotency by culturing them for two passages in LIF plus Gsk3β (CHIR99021 or Chiron)
688 and MEK (PD0325091) inhibitors (2i/LIF). mESCs were further differentiated towards the
689 primed pluripotent state (epiblast-like cells) by culturing mESCs in a medium containing
690 20ng/mL Activin A and 10ng/mL Fgf2 for 120h. **B-C.** Relative mRNA levels (based on qPCR
691 experiments) of the canonical IκB genes (*Nfkbia, Nfkbib, Nfkbie*) (**B**) or Nf-κB effector genes
692 (*Rela, c-Rel, Relb, Nfkb1, Nfkb2*) (**C**) across the different states of pluripotency. Expression was
693 normalized using the house-keeping gene *Tbp* relative to 2i/LIF. Data from three independent
694 experiments. Dots indicate mean values and error bars refer to ± standard deviation (SD). **D.**
695 Western blot analysis of IκBα protein distribution in cytoplasm, nucleoplasm (Nucleus) or
696 chromatin in cells at the ground-state of naïve pluripotency (2i/L), naïve pluripotency (S/L) or
697 primed pluripotency (Epi). This experiment was independently repeated twice. **E.**
698 Transcriptome and proteome differences across naïve (2i/LIF) and primed (Epiblast-like cells
699 or EpiSCs) pluripotent states. Enriched transcripts and proteins in naïve state are highlighted
700 in red (Log_2 fold-change < -1). Enriched transcripts and proteins in the primed state are
701 marked in dark gray (Log_2 fold-change > 1). Data from [33]. **F.** Heatmap showing the expression
702 levels of pluripotency (*Dppa4, Pou5f1, Sox2, Prdm14, Klf4, Zfp42, Nanog*), differentiation
703 (*Mesp1, Gata4, Gata6, Lhx1, Wnt3a, Fgf5, Nes, Axin2, Wnt3, Eomes, Foxa2, T, Mixl1, Lef1*) NF-
704 κB (*Nfkbia, Nfkbib, Nfkbie, Nfkbiz, Rela, c-Rel, Relb*) and Polycomb (*Ezh1, Ezh2, Eed, Epop,*
705 *Jarid2, Suz12, Mtf2, Aebp2*) genes from the RNAseq samples at mESCs (Serum/LIF) and
706 differentiating cells (embryoid bodies) at 48h and 96h of IκBα-WT cells. Normalized counts
707 based on z-score are represented.

708 **Figure 2. The absence of IκBα hinders the exit from the pluripotent state and prevents the**
709 **activation of differentiation programs. A.** Representative immunofluorescence of 216h EBs
710 stained with the pluripotency markers NANOG and OCT3/4. **B.** Quantification of total number
711 of alkaline phosphatase (AP) colonies after 216h EB differentiation and additional culture of
712 96h in Serum/LIF (S/L) medium. Dots represent values from two independent experiments
713 from three different IκBα-WT or IκBα-KO clones. Unpaired two-sided t-test applied.
714 Representative images from AP colonies are included in the upper panel. **C.** PC1 and PC2 from
715 Principal Component Analysis (PCA) of normalized RNA-seq data from 3 different time points
716 (mESCs, 48h EBs and 96h EBs) of IκBα-WT and IκBα-KO cells (three independent clones from
717 each genotype). **D.** Heatmap showing the expression levels of naïve pluripotency genes
718 (*Gab1, Sox2, Esrrb, Zfp42, Dppa4, Klf2, Prdm14, Klf4, Tfcp2l1*) from the RNAseq samples of
719 IκBα-WT and IκBα-KO EBs at 96h. Normalized counts based on z-score are represented. **E**. Z-
720 score values for gene sets referring to Endoderm, Mesoderm and Ectoderm formation from
721 The Gene Ontology database (GO:0001706, GO:0001707 and GO:0001705 terms,
722 respectively) and obtained from corresponding expression levels at mESCs, 48h and 96h EBs

723 IκBα-WT or IκBα-KO cells (three independent clones of each genotype). Loess curves are also
724 represented with 95% confidence intervals (shadowed area surrounding the curves). **F.**
725 Schematic of teratoma formation assay. $5x10^5$ IκBα-WT or IκBα-KO mESCs cultured in
726 Serum/LIF were injected intramuscularly in the leg of immunocompromised NSG mice. 6
727 weeks after the transplant, teratomas were formed, and mice were euthanized for further
728 teratoma analysis. **G.** Representative images of immunohistochemistry for OCT3/4 in IκBα-
729 WT (left panel) or IκBα-KO (right panel) teratomas. Teratomas were derived from three
730 independent clones of mESCs of both genotypes. **H.** Percentage of $OCT3/4^+$ cells in teratomas.
731 Positive cells were counted from five different microscope fields from each IκBα-WT and IκBα-
732 KO clone. Unpaired two-sided t-test was performed. Bars indicate mean values and error bars
733 refer to ± SD.

734 **Figure 3. IκBα-KO mESCs retain the ground-state of naïve pluripotency under Serum/LIF**
735 **culture. A.** (Upper panel) Schematics of mESCs differentiation towards Epiblast Stem Cells
736 (EpiSCs). mESCs cultured in Serum/LIF were then seeded in N2B27 medium supplemented
737 with 10ng/mL Fgf2 and 20ng/mL Activin A for 120h (see Materials and Methods section for
738 further information). (Bottom panel) Relative RNA levels (based on qPCR experiments) of
739 naïve pluripotency genes (*Nanog, Sox2, Rex1, Klf4, Gbx2, Tbx3, Dppa3*) in IκBα-WT or IκBα-KO
740 EpiSCs at 120h. RNA levels were normalized based on *Tbp* expression relative to IκBα-WT.
741 Each dot represents an independent clone either from IκBα-WT or IκBα-KO genotypes.
742 Unpaired two-sided t-test applied. Horizontal bars indicate mean values and error bars refer
743 to ± SD. **B.** GSEA results comparing IκBα-KO vs IκBα-WT mESCs cultured in Serum/LIF against
744 ground (2i/LIF) and naïve (Serum/LIF) state pluripotency signatures retrieved from [35].
745 Adjusted p-value by Benjamini-Hochberg procedure and Normalized Enrichment Score (NES)
746 indicated. **C.** Relative RNA levels of the naïve pluripotency genes *Rex1 (Zfp42), Klf2* and *Tbx3*
747 upon culture of IκBα-WT either in Serum/LIF or two passages in 2i/LIF. 2i/LIF IκBα-WT mESCs
748 were compared with IκBα-KO mESCs cultured in Serum/LIF. Unpaired two-sided t-test was
749 applied to calculate statistical significance. Each dot represents an independent clone from
750 each of the two genotypes. **D.** Representative immunofluorescence images of DNA-
751 methylation-related mark 5-methylcytosine (5mC) in IκBα-WT (left) and IκBα-KO (right)
752 mESCs cultured in Serum/LIF. **E.** DNA methylation profile (using DNA methylation arrays [36]) in
753 IκBα-WT vs IκBα-KO mESCs (upper) and 96h EBs (bottom panel) showing the distribution
754 density of mean ß-values from all 261,220 CpGs under test per condition.

755 **Figure 4. Absence of IκBα reinforces the pluripotency program at the epigenetic and**
756 **transcriptional levels. A.** ChIP-seq Enrichment Analysis (ChEA) of differentially expressed
757 genes (DEGs; adjusted p-value<0.05) in IκBα-KO mESCs. P-value was calculated using Fisher
758 exact test. **B.** Number of differentially bound regions (adjusted p-value <0.05, FDR) for
759 H3K4me3 and H3K27me3 histone marks in IκBα $^{-/-}$ vs IκBα $^{+/+}$ mESCs cultured in Serum/LIF.
760 Enriched or reduced regions in IκBα $^{-/-}$ mESCs are distinguished (log_2 Fold-change >0 or <0,
761 respectively). Overrepresented WikiPathways, for (left) H3K4me3 and (right) H3K27me3 are
762 indicated. Annotated genes to differential regions showing H3K4me3 enrichment or

763 H3K27me3 reduction were considered. A one-sided hypergeometric test was conducted. **C.**
764 Venn Diagram of genes contained in regions with either increased H3K4me3 or reduced levels
765 of H3K27me3. Statistical significance of the overlapping was calculated using the chi-squared
766 method. Overrepresented pathways for genes containing increased H3K4me3 and reduced
767 H3K27me3 levels are indicated (only pathways with an adjusted p-value<0.05 were
768 considered). **D-E.** Representative genomic regions of naïve pluripotency genes having either
769 differential enriched H3K4me3-only (D) or reduced H3K27me3-only (E) levels in IκBα-KO vs
770 IκBα-WT mESCs cultured in Serum/LIF. Shadowed regions highlight the differential levels of
771 the histone marks. **F.** Number of regions with differential enhancer activity in IκBα-KO vs IκBα-
772 WT mESCs cultured in Serum/LIF. Increased/Reduced activity for (left) poised enhancers
773 based on the H3K4me1 differential binding and absence of H3K27ac overlapping peaks in
774 IκBα-KO mESCs and, (right) active enhancers based on the differential binding of H3K27ac
775 and presence of H3K4me1 overlapping peaks in IκBα-KO. Differential binding based on
776 adjusted p-value <0.05 (FDR). Increased or reduced regions in IκBα-KO are distinguished by
777 log_2 Fold-change >0 or <0, respectively, compared to IκBα-WT mESCs. Overrepresented
778 WikiPathways for annotated genes to (left) poised enhancers with reduced activity and (right)
779 active enhancers with increased activity in IκBα-KO vs IκBα-WT mESCs are indicated
780 (adjusted p-value < 0.05, FDR). A one-sided hypergeometric test was conducted. **G.**
781 Representative genomic regions of naïve pluripotency genes having an increase in active
782 enhancer status (H3K27Ac enrichment) in IκBα-KO mESCs cultured in Serum/LIF. Shadowed
783 regions highlight the differential levels of the histone mark. **H.** Heatmap showing the
784 expression levels of the naïve pluripotency genes from the RNAseq samples of IκBα-KO and
785 IκBα-WT mESCs cultured in Serum/LIF. Normalized counts (z-score) from genes are
786 represented.

787 **Figure 5. IκBα prevents the hyperactivation of naïve pluripotency program in an NF-κB-**
788 **independent manner. A.** Boxplots, violin plots and individual values representing the
789 normalized gene expression levels in IκBα-WT or IκBα-KO mESCs, EBs 48h and EBs 96h.
790 Considered genes are those annotated to NF-κB signaling pathway (KEGG PATHWAY
791 mmu04064). Box Plots: center line, median; lower and upper hinges, first and third quartiles;
792 whiskers, 1.5x interquartile range (IQR) extended to the largest/smallest value within 1.5xIQR;
793 no outliers present. Unpaired two-sided Wilcoxon test applied. **B.** Schematic of chromatin-
794 specific/NF-κB-deficient (IκBα$^{\Delta NF\text{-}\kappa B}$) or NF-κB-specific/chromatin-deficient (IκBα$^{\Delta Chrom}$) IκBα
795 mutants (Separation-Of-Function or SOF mutants). **C.** Pull-down of GST-H2A and GST-P50 with
796 cell lysates from different SOF IκBα mutant mESCs. **D.** Western blot analysis of cytoplasmic
797 protein extracts of doxycycline-inducible IκBα forms (i-IκBα$^{\Delta WT}$, i-IκBα$^{\Delta NF\text{-}\kappa B}$, i-IκBα$^{\Delta Chrom}$) after
798 16h of doxycycline induction. **E.** Western blot analysis of chromatin protein extracts of
799 doxycycline-inducible IκBα forms (i-IκBα$^{\Delta WT}$, i-IκBα$^{\Delta NF\text{-}\kappa B}$, IκBα$^{\Delta Chrom}$) after 16h of doxycycline
800 induction. **F.** Relative RNA levels of naïve pluripotency genes (*Zfp42, Klf2, Sox2, Tbx3*) in i-
801 IκBα^{WT}, i-IκBα$^{\Delta NF\text{-}\kappa B}$ and i-IκBα$^{\Delta Chrom}$ mESCs after doxycycline induction. Unpaired two-sided t-
802 test was performed. Bars indicate mean values and error bars refer to ± SEM. **G.**

803 Representative immunofluorescence images of DNA-methylation-related mark 5-
804 methylcytosine (5mC) in i-IκBα$^{\Delta WT}$ (upper panel), i-IκBα$^{\Delta NF\text{-}\kappa B}$ (medium panel), IκBα$^{\Delta Chrom}$
805 (bottom panel) mESCs cultured in Serum/LIF. **H.** Flow cytometry analysis of the pluripotency
806 surface marker SSEA-1 at 216h EBs in i-IκBα^{WT}, i-IκBα$^{\Delta NF\text{-}\kappa B}$ and i-IκBα$^{\Delta Chrom}$ cells. **I.**
807 Quantification of Alkaline Phosphatase (AP) staining in 216h EBs upon reconstitution with the
808 different IκBα forms. Each dot represents an independent experiment. One-way ANOVA was
809 applied. Bars indicate mean values and error bars refer to ± SEM. Representative images of
810 Alkaline Phosphatase (AP) staining in 216h EBs are included in the upper panel. **J.**
811 Representative immunofluorescence for NANOG and OCT3/4 at 216h EBs in i-IκBα^{WT} (upper
812 panel), i-IκBα$^{\Delta NF\text{-}\kappa B}$ (medium panel) and i-IκBα$^{\Delta Chrom}$ (bottom panel) cells.

813 **Figure S1. Depletion of IκBα in mESCs compromises the exit from pluripotency. Related to**
814 **Figure 2. A.** Schematic of the approach followed to deplete IκBα protein in mESCs (upper
815 panel) and western blot analysis of three independent IκBα-WT and IκBα-KO mESC clones
816 (bottom panel). **B.** Volcano plot from differential expression analysis between IκBα-KO vs
817 IκBα-WT 96h EBs. Dashed vertical lines represent an absolute shrunken $\log_2$ Fold Change = 1
818 and dashed horizontal line represents an adjusted p-value = 0.05 (FDR). **C.** Flow cytometry
819 plots of SSEA-1 from IκBα-WT or IκBα-KO EBs 216h. **D.** Schematic of Alkaline Phosphatase (AP)
820 staining carried out in EBs. IκBα-WT or IκBα-KO 216h EBs were dissociated and seeded in
821 Serum/LIF medium for another 96h. Attached cells were screened for AP^+ total cell number.
822 **E.** Violin plot and individual values showing the quantification of relative size of 168h EBs.
823 Each dot represents an embryoid body. Unpaired two-sided t-test was applied. **F.** Relative
824 RNA levels of naïve pluripotency genes (*Pou5f1, Gbx2, Klf2, Sox2, Rex1, Nanog*) in IκBα-WT or
825 IκBα-KO 216h EBs. RNA levels were normalized based on *Tbp* expression relative to IκBα-WT.
826 Each dot represents an independent clone either from IκBα-WT or IκBα-KO genotypes.
827 Unpaired two-sided t-test was applied. **G.** Relative RNA levels of differentiation genes (*Mixl1,*
828 *Mesp1, T, KDR, Gata6, Zic1*) in IκBα-WT or IκBα-KO 216h EBs. RNA levels were normalized
829 based on *Tbp* expression relative to IκBα-WT. Each dot represents an independent clone
830 either from IκBα-WT or IκBα-KO genotypes.

831 **Figure S2. Absence of IκBα favors the ground-state of naïve pluripotency in Serum/LIF**
832 **conditions. Related to Figure 3. A.** Brightfield images of IκBα-WT or IκBα-KO EpiSCs at 120h.
833 Each picture corresponds to an independent clone from either IκBα-WT or IκBα-KO
834 genotypes. **B.** Bright-field microscopy images of IκBα-WT and IκBα-KO mESCs cultured in
835 Serum/LIF conditions. Two independent clones from each genotype are shown. **C.** DNA
836 methylation levels (mean ß-values) across chromosomes in IκBα-WT vs IκBα-KO mESCs.

837 **Figure S3. Epigenetic rewiring characterization in IκBα-KO mESCs cultured in Serum/LIF.**
838 **Related to Figure 4. A-D.** Volcano plots from differential binding analysis of H3K4me3 (A),
839 H3K27me3 (B), H3K4me1 (C) and H3K27Ac (D) in IκBα-WT vs IκBα-KO mESCs cultured in
840 Serum/LIF. Representative genes with enriched or reduced levels of H3K4me3 (A), H3K27me3
841 (B), H3K4me1 (C) and H3K27Ac (D) marks in IκBα-KO mESCs are highlighted. E-F.

842 Representative genomic regions of naïve pluripotency genes having higher H3K4me3 (E) or
843 reduced H3K27me3 (F) levels in 2i/LIF compared to Serum/LIF medium. Displayed regions are
844 the ones having differential H3K4me3 and H3K27me3 distribution in IκBα-WT vs IκBα-KO
845 mESCs. Shadowed regions highlight the differential levels of the histone marks. Data from
846 Galonska et al 2015.

847 **Figure S4. Reversion of IκBα-KO-related hyper pluripotent status is NF-κB independent.**
848 **Related to Figure 5. A.** Relative expression level of Nfkbia gene after overnight doxycycline
849 induction in i-IκBα$^{\Delta WT}$, i-IκBα$^{\Delta NF\text{-}\kappa B}$ and IκBα$^{\Delta Chrom}$ mESCs. **B.** Schematic representation of
850 reconstitution of IκBα-KO mESCs with either of the two doxycycline-inducible SOF mutants (i-
851 IκBα$^{\Delta NF\text{-}\kappa B}$ or IκBα$^{\Delta Chrom}$). mESCs were then kept in Serum/LIF medium supplemented with
852 1µg/mL Doxycycline for 4 consecutive passages. mESCs were characterized at the pluripotent
853 level and then their potential to be further differentiated was addressed. **C.** Percentage of
854 differentiated cells (determined as SSEA-1.) at 216h EBs 216h derived from i-IκBα$^{\Delta WT}$, i-
855 IκBα$^{\Delta NF\text{-}\kappa B}$ and IκBα$^{\Delta Chrom}$ mESCs. **D.** Quantification of EB differentiation status (percentage of
856 pluripotent cells) at 216h after induction of SOF IκBα mutants. Data from three independent
857 experiments. **E.** Representative immunofluorescence for NANOG and OCT3/4 at 216h EBs that
858 have not been treated with doxycycline in i-IκBα^{WT} (upper panel), i-IκBα$^{\Delta NF\text{-}\kappa B}$ (medium) and i-
859 IκBα$^{\Delta Chrom}$ (bottom) cells.

860 **REFERENCES**

861 1. Festuccia, N., Osorno, R., Wilson, V., and Chambers, I. (2013). The role of pluripotency
862 gene regulatory network components in mediating transitions between pluripotent cell
863 states. Curr. Opin. Genet. Dev. *23*, 504–511.

864 2. Graf, T., and Stadtfeld, M. (2008). Heterogeneity of embryonic and adult stem cells. Cell
865 Stem Cell *3*, 480–483.

866 3. Martinez Arias, A., and Brickman, J.M. (2011). Gene expression heterogeneities in
867 embryonic stem cell populations: origin and function. Curr. Opin. Cell Biol. *23*, 650–656.

868 4. Pera, M.F., and Rossant, J. (2021). The exploration of pluripotency space: Charting cell
869 state transitions in peri-implantation development. Cell Stem Cell *28*, 1896–1906.

870 5. Wang, X., and Wu, Q. (2022). The Divergent Pluripotent States in Mouse and Human
871 Cells. Genes *13*. 10.3390/genes13081459.

872 6. Ying, Q.-L., Wray, J., Nichols, J., Batlle-Morera, L., Doble, B., Woodgett, J., Cohen, P.,
873 and Smith, A. (2008). The ground state of embryonic stem cell self-renewal. Nature
874 *453*, 519–523.

875 7. Marks, H., Kalkan, T., Menafra, R., Denissov, S., Jones, K., Hofemeister, H., Nichols, J.,
876 Kranz, A., Stewart, A.F., Smith, A., et al. (2012). The transcriptional and epigenomic
877 foundations of ground state pluripotency. Cell *149*, 590–604.

878 8. Boroviak, T., Loos, R., Lombard, P., Okahara, J., Behr, R., Sasaki, E., Nichols, J., Smith, A.,
879 and Bertone, P. (2015). Lineage-Specific Profiling Delineates the Emergence and
880 Progression of Naive Pluripotency in Mammalian Embryogenesis. Dev. Cell *35*, 366–
881 382.

882 9. Brons, I.G.M., Smithers, L.E., Trotter, M.W.B., Rugg-Gunn, P., Sun, B., Chuva de Sousa
883 Lopes, S.M., Howlett, S.K., Clarkson, A., Ahrlund-Richter, L., Pedersen, R.A., et al.
884 (2007). Derivation of pluripotent epiblast stem cells from mammalian embryos. Nature
885 *448*, 191–195.

886 10. Tesar, P.J., Chenoweth, J.G., Brook, F.A., Davies, T.J., Evans, E.P., Mack, D.L., Gardner,
887 R.L., and McKay, R.D.G. (2007). New cell lines from mouse epiblast share defining
888 features with human embryonic stem cells. Nature *448*, 196–199.

889 11. Weinberger, L., Ayyash, M., Novershtern, N., and Hanna, J.H. (2016). Dynamic stem cell
890 states: naive to primed pluripotency in rodents and humans. Nat. Rev. Mol. Cell Biol.
891 *17*, 155–169.

892 12. Guo, G., Yang, J., Nichols, J., Hall, J.S., Eyres, I., Mansfield, W., and Smith, A. (2009). Klf4
893 reverts developmentally programmed restriction of ground state pluripotency.
894 Development *136*, 1063–1069.

895 13. Takahashi, S., Kobayashi, S., and Hiratani, I. (2018). Epigenetic differences between

896 naïve and primed pluripotent stem cells. Cell. Mol. Life Sci. *75*, 1191–1203.

897 14. Bao, S., Tang, F., Li, X., Hayashi, K., Gillich, A., Lao, K., and Surani, M.A. (2009).
898 Epigenetic reversion of post-implantation epiblast to pluripotent embryonic stem cells.
899 Nature *461*, 1292–1295.

900 15. Habibi, E., Brinkman, A.B., Arand, J., Kroeze, L.I., Kerstens, H.H.D., Matarese, F.,
901 Lepikhov, K., Gut, M., Brun-Heath, I., Hubner, N.C., et al. (2013). Whole-genome
902 bisulfite sequencing of two distinct interconvertible DNA methylomes of mouse
903 embryonic stem cells. Cell Stem Cell *13*, 360–369.

904 16. Leitch, H.G., McEwen, K.R., Turp, A., Encheva, V., Carroll, T., Grabole, N., Mansfield, W.,
905 Nashun, B., Knezovich, J.G., Smith, A., et al. (2013). Naive pluripotency is associated
906 with global DNA hypomethylation. Nat. Struct. Mol. Biol. *20*, 311–316.

907 17. Singer, Z.S., Yong, J., Tischler, J., Hackett, J.A., Altinok, A., Surani, M.A., Cai, L., and
908 Elowitz, M.B. (2014). Dynamic heterogeneity and DNA methylation in embryonic stem
909 cells. Mol. Cell *55*, 319–331.

910 18. Factor, D.C., Corradin, O., Zentner, G.E., Saiakhova, A., Song, L., Chenoweth, J.G.,
911 McKay, R.D., Crawford, G.E., Scacheri, P.C., and Tesar, P.J. (2014). Epigenomic
912 comparison reveals activation of "seed" enhancers during transition from naive to
913 primed pluripotency. Cell Stem Cell *14*, 854–863.

914 19. Buecker, C., Srinivasan, R., Wu, Z., Calo, E., Acampora, D., Faial, T., Simeone, A., Tan,
915 M., Swigut, T., and Wysocka, J. (2014). Reorganization of enhancer patterns in
916 transition from naive to primed pluripotency. Cell Stem Cell *14*, 838–853.

917 20. Gerondakis, S., Grumont, R., Gugasyan, R., Wong, L., Isomura, I., Ho, W., and Banerjee,
918 A. (2006). Unravelling the complexities of the NF-kappaB signalling pathway using
919 mouse knockout and transgenic models. Oncogene *25*, 6781–6799.

920 21. Kaltschmidt, C., Greiner, J.F.W., and Kaltschmidt, B. (2021). The Transcription Factor
921 NF-κB in Stem Cells and Development. Cells *10*. 10.3390/cells10082042.

922 22. Espín-Palazón, R., and Traver, D. (2016). The NF-κB family: Key players during
923 embryonic development and HSC emergence. Exp. Hematol. *44*, 519–527.

924 23. Li, S., Sun, J., Zhang, B.-W., Yang, L., Wan, Y.-C., Chen, B.-B., Xu, N., Xu, Q.-R., Fan, J.,
925 Shang, J.-N., et al. (2024). ATG5 attenuates inflammatory signaling in mouse embryonic
926 stem cells to control differentiation. Dev. Cell. 10.1016/j.devcel.2024.01.026.

927 24. Torres, J., and Watt, F.M. (2008). Nanog maintains pluripotency of mouse embryonic
928 stem cells by inhibiting NFkappaB and cooperating with Stat3. Nat. Cell Biol. *10*, 194–
929 201.

930 25. Dutta, D., Ray, S., Home, P., Larson, M., Wolfe, M.W., and Paul, S. (2011). Self-renewal
931 versus lineage commitment of embryonic stem cells: protein kinase C signaling shifts
932 the balance. Stem Cells *29*, 618–628.

933 26. Zhang, Q., Lenardo, M.J., and Baltimore, D. (2017). 30 Years of NF-κB: A Blossoming of
934 Relevance to Human Pathobiology. Cell *168*, 37–57.

935 27. Mulero, M.C., Ferres-Marco, D., Islam, A., Margalef, P., Pecoraro, M., Toll, A., Drechsel,
936 N., Charneco, C., Davis, S., Bellora, N., et al. (2013). Chromatin-bound IκBα regulates a
937 subset of polycomb target genes in differentiation and cancer. Cancer Cell *24*, 151–166.

938 28. Marruecos, L., Bertran, J., Guillén, Y., González, J., Batlle, R., López-Arribillaga, E.,
939 Garrido, M., Ruiz-Herguido, C., Lisiero, D., González-Farré, M., et al. (2020). IκBα
940 deficiency imposes a fetal phenotype to intestinal stem cells. EMBO Rep. *21*, e49708.

941 29. Marruecos, L., Bertran, J., Álvarez-Villanueva, D., Mulero, M.C., Guillén, Y., Palma, L.G.,
942 Floor, M., Vert, A., Arce-Gallego, S., Pecharroman, I., et al. (2021). Dynamic chromatin
943 association of IκBα is regulated by acetylation and cleavage of histone H4. EMBO Rep.
944 *22*, e52649.

945 30. Thambyrajah, R., Maqueda, M., Fadlullah, M.Z., Proffitt, M., Neo, W.H., Guillén, Y.,
946 Casado-Pelaez, M., Herrero-Molinero, P., Brujas, C., Castelluccio, N., et al. (2024). IκBα
947 controls dormancy in hematopoietic stem cells via retinoic acid during embryonic
948 development. Nat. Commun. *15*, 4673.

949 31. Aguilera, C., Hoya-Arias, R., Haegeman, G., Espinosa, L., and Bigas, A. (2004).
950 Recruitment of IκBα to the *hes1* promoter is associated with transcriptional repression.
951 Proceedings of the National Academy of Sciences *101*, 16537–16542.

952 32. Alvarez-Villanueva, D., Galan, L., Bertran, J., and Floor, M. (2023). Separation-of-
953 function mutants reveal the NF-κB-independent involvement of IκBα in the regulation
954 of stem cell and oncogenic programs. bioRxiv.

955 33. Atlasi, Y., Jafarnejad, S.M., Gkogkas, C.G., Vermeulen, M., Sonenberg, N., and
956 Stunnenberg, H.G. (2020). The translational landscape of ground state pluripotency.
957 Nat. Commun. *11*, 1617.

958 34. Tian, T.V., Di Stefano, B., Stik, G., Vila-Casadesús, M., Sardina, J.L., Vidal, E., Dasti, A.,
959 Segura-Morales, C., De Andrés-Aguayo, L., Gómez, A., et al. (2019). Whsc1 links
960 pluripotency exit with mesendoderm specification. Nat. Cell Biol. *21*, 824–834.

961 35. Ghimire, S., Van der Jeught, M., Neupane, J., Roost, M.S., Anckaert, J., Popovic, M., Van
962 Nieuwerburgh, F., Mestdagh, P., Vandesompele, J., Deforce, D., et al. (2018).
963 Comparative analysis of naive, primed and ground state pluripotency in mouse
964 embryonic stem cells originating from the same genetic background. Sci. Rep. *8*, 5884.

965 36. Zhou, W., Hinoue, T., Barnes, B., Mitchell, O., Iqbal, W., Lee, S.M., Foy, K.K., Lee, K.-H.,
966 Moyer, E.J., VanderArk, A., et al. (2022). DNA methylation dynamics and dysregulation
967 delineated by high-throughput profiling in the mouse. Cell Genom *2*.
968 10.1016/j.xgen.2022.100144.

969 37. Choi, J., Huebner, A.J., Clement, K., Walsh, R.M., Savol, A., Lin, K., Gu, H., Di Stefano, B.,
970 Brumbaugh, J., Kim, S.-Y., et al. (2017). Prolonged Mek1/2 suppression impairs the

971 developmental potential of embryonic stem cells. Nature *548*, 219–223.

972 38. Di Stefano, B., Luo, E.-C., Haggerty, C., Aigner, S., Charlton, J., Brumbaugh, J., Ji, F.,
973 Rabano Jiménez, I., Clowers, K.J., Huebner, A.J., et al. (2019). The RNA Helicase DDX6
974 Controls Cellular Plasticity by Modulating P-Body Homeostasis. Cell Stem Cell *25*, 622–
975 638.e13.

976 39. Brena, D., Bertran, J., Porta-de-la-Riva, M., Guillén, Y., Cornes, E., Kukhtar, D., Campos-
977 Vicens, L., Fernández, L., Pecharroman, I., García-López, A., et al. (2020). Ancestral
978 function of Inhibitors-of-kappaB regulates Caenorhabditis elegans development. Sci.
979 Rep. *10*, 16153.

980 40. Hayden, M.S., and Ghosh, S. (2008). Shared principles in NF-kappaB signaling. Cell *132*,
981 344–362.

982 41. Basak, S., Kim, H., Kearns, J.D., Tergaonkar, V., O'Dea, E., Werner, S.L., Benedict, C.A.,
983 Ware, C.F., Ghosh, G., Verma, I.M., et al. (2007). A fourth IkappaB protein within the
984 NF-kappaB signaling module. Cell *128*, 369–381.

985 42. Thambyrajah, R., Fadlullah, Z., Proffitt, M., Neo, W.H., Guillén, Y., Casado-Pelaez, M.,
986 Herrero-Molinero, P., Brujas, C., Castelluccio, N., González, J., et al. (2022). IκBα
987 controls dormancy induction in Hematopoietic stem cell development via retinoic acid.
988 bioRxiv, 2022.11.17.516971. 10.1101/2022.11.17.516971.

989 43. Álvarez-Villanueva, D., Galán-Palma, L., Bertran, J., Floor, M., Solé, L., Lobo-Jarne, T.,
990 Maqueda, M., Rajbhandari, R., Marruecos, L., Villà-Freixa, J., et al. (2023). Separation-
991 of-function mutants reveal the NF-κB-independent involvement of IκBα in the
992 regulation of stem cell and oncogenic programs. bioRxiv, 2023.06.21.545928.
993 10.1101/2023.06.21.545928.

994 44. Guo, Y.-L. (2019). The underdeveloped innate immunity in embryonic stem cells: The
995 molecular basis and biological perspectives from early embryogenesis. Am. J. Reprod.
996 Immunol. *81*, e13089.

997 45. Pantier, R., Tatar, T., Colby, D., and Chambers, I. (2019). Endogenous epitope-tagging of
998 Tet1, Tet2 and Tet3 identifies TET2 as a naïve pluripotency marker. Life Sci Alliance *2*.
999 10.26508/lsa.201900516.

1000 46. Sroczynska, P., Lancrin, C., Pearson, S., Kouskoff, V., and Lacaud, G. (2009). In vitro
1001 differentiation of mouse embryonic stem cells as a model of early hematopoietic
1002 development. Methods Mol. Biol. *538*, 317–334.

1003 47. Chen, Q., Luo, W., Veach, R.A., Hickman, A.B., Wilson, M.H., and Dyda, F. (2020).
1004 Structural basis of seamless excision and specific targeting by piggyBac transposase.
1005 Nat. Commun. *11*, 3446.

1006 48. Schneider, C.A., Rasband, W.S., and Eliceiri, K.W. (2012). NIH Image to ImageJ: 25 years
1007 of image analysis. Nat. Methods *9*, 671–675.

1008 49. Ewels, P., Afyounian, E., and Schuster-Boeckler, B.F.K. (2012). TrimGalore: v0. 6.7-DOI
1009 via Zenodo.(Zenodo, 2021). doi: 10.5281/zenodo. 5127899. 2. Langmead, B. & Salzberg,
1010 SL Fast gapped-read alignment with …. Nat. Methods.

1011 50. Langmead, B., and Salzberg, S.L. (2012). Fast gapped-read alignment with Bowtie 2.
1012 Nat. Methods *9*, 357–359.

1013 51. Danecek, P., Bonfield, J.K., Liddle, J., Marshall, J., Ohan, V., Pollard, M.O., Whitwham,
1014 A., Keane, T., McCarthy, S.A., Davies, R.M., et al. (2021). Twelve years of SAMtools and
1015 BCFtools. Gigascience *10*. 10.1093/gigascience/giab008.

1016 52. Landt, S.G., Marinov, G.K., Kundaje, A., Kheradpour, P., Pauli, F., Batzoglou, S.,
1017 Bernstein, B.E., Bickel, P., Brown, J.B., Cayting, P., et al. (2012). ChIP-seq guidelines and
1018 practices of the ENCODE and modENCODE consortia. Genome Res. *22*, 1813–1831.

1019 53. Ramírez, F., Ryan, D.P., Grüning, B., Bhardwaj, V., Kilpert, F., Richter, A.S., Heyne, S.,
1020 Dündar, F., and Manke, T. (2016). deepTools2: a next generation web server for deep-
1021 sequencing data analysis. Nucleic Acids Res. *44*, W160–W165.

1022 54. Stovner, E.B., and Sætrom, P. (2019). epic2 efficiently finds diffuse domains in ChIP-seq
1023 data. Bioinformatics *35*, 4392–4393.

1024 55. Zhang, Y., Liu, T., Meyer, C.A., Eeckhoute, J., Johnson, D.S., Bernstein, B.E., Nusbaum,
1025 C., Myers, R.M., Brown, M., Li, W., et al. (2008). Model-based analysis of ChIP-Seq
1026 (MACS). Genome Biol. *9*, R137.

1027 56. Stark, R., Brown, G., and Others (2011). DiffBind: differential binding analysis of ChIP-
1028 Seq peak data. R package version *100*.

1029 57. Gu, Z., Eils, R., Schlesner, M., and Ishaque, N. (2018). EnrichedHeatmap: an
1030 R/Bioconductor package for comprehensive visualization of genomic signal
1031 associations. BMC Genomics *19*, 234.

1032 58. Robinson, J.T., Thorvaldsdóttir, H., Winckler, W., Guttman, M., Lander, E.S., Getz, G.,
1033 and Mesirov, J.P. (2011). Integrative genomics viewer. Nat. Biotechnol. *29*, 24–26.

1034 59. Liao, Y., Smyth, G.K., and Shi, W. (2014). featureCounts: an efficient general purpose
1035 program for assigning sequence reads to genomic features. Bioinformatics *30*, 923–
1036 930.

1037 60. Love, M.I., Huber, W., and Anders, S. (2014). Moderated estimation of fold change and
1038 dispersion for RNA-seq data with DESeq2. Genome Biol. *15*, 550.

1039 61. Zhu, A., Ibrahim, J.G., and Love, M.I. (2019). Heavy-tailed prior distributions for
1040 sequence count data: removing the noise and preserving large differences.
1041 Bioinformatics *35*, 2084–2092.

1042 62. Benjamini, Y., and Hochberg, Y. (1995). Controlling the False Discovery Rate: A Practical
1043 and Powerful Approach to Multiple Testing. J. R. Stat. Soc. Series B Stat. Methodol. *57*,

1044 289–300.

1045 63. Garcia-Prieto, C.A., Álvarez-Errico, D., Musulen, E., Bueno-Costa, A., N. Vazquez, B.,
1046 Vaquero, A., and Esteller, M. (2022). Validation of a DNA methylation microarray for
1047 285,000 CpG sites in the mouse genome. Epigenetics *17*, 1677–1685.

1048 64. Ashburner, M., Ball, C.A., Blake, J.A., Botstein, D., Butler, H., Cherry, J.M., Davis, A.P.,
1049 Dolinski, K., Dwight, S.S., Eppig, J.T., et al. (2000). Gene ontology: tool for the
1050 unification of biology. The Gene Ontology Consortium. Nat. Genet. *25*, 25–29.

1051 65. Kanehisa, M., and Goto, S. (2000). KEGG: kyoto encyclopedia of genes and genomes.
1052 Nucleic Acids Res. *28*, 27–30.

1053 66. Martens, M., Ammar, A., Riutta, A., Waagmeester, A., Slenter, D.N., Hanspers, K., A
1054 Miller, R., Digles, D., Lopes, E.N., Ehrhart, F., et al. (2021). WikiPathways: connecting
1055 communities. Nucleic Acids Res. *49*, D613–D621.

1056 67. Hu, S., Metcalf, E., Mahat, D.B., Chan, L., Sohal, N., Chakraborty, M., Hamilton, M.,
1057 Singh, A., Singh, A., Lees, J.A., et al. (2022). Transcription factor antagonism regulates
1058 heterogeneity in embryonic stem cell states. Mol. Cell *82*, 4410–4427.e12.

1059 68. Korotkevich, G., Sukhov, V., Budin, N., Shpak, B., Artyomov, M.N., and Sergushichev, A.
1060 (2021). Fast gene set enrichment analysis. bioRxiv, 060012. 10.1101/060012.

1061 69. Zhou, W., Triche, T.J., Jr, Laird, P.W., and Shen, H. (2018). SeSAMe: reducing artifactual
1062 detection of DNA methylation by Infinium BeadChips in genomic deletions. Nucleic
1063 Acids Res. *46*, e123.

1064 70. Hänzelmann, S., Castelo, R., and Guinney, J. (2013). GSVA: gene set variation analysis
1065 for microarray and RNA-seq data. BMC Bioinformatics *14*, 7.

1066 71. Galonska, C., Ziller, M.J., Karnik, R. and Meissner, A. (2015) Ground State conditions
1067 induce rapid reorganization of core pluripotency factor birnding before global epigenetic
1068 reprogramming. Cell Stem Cell, 17, 4, 462-470.

Figure 1

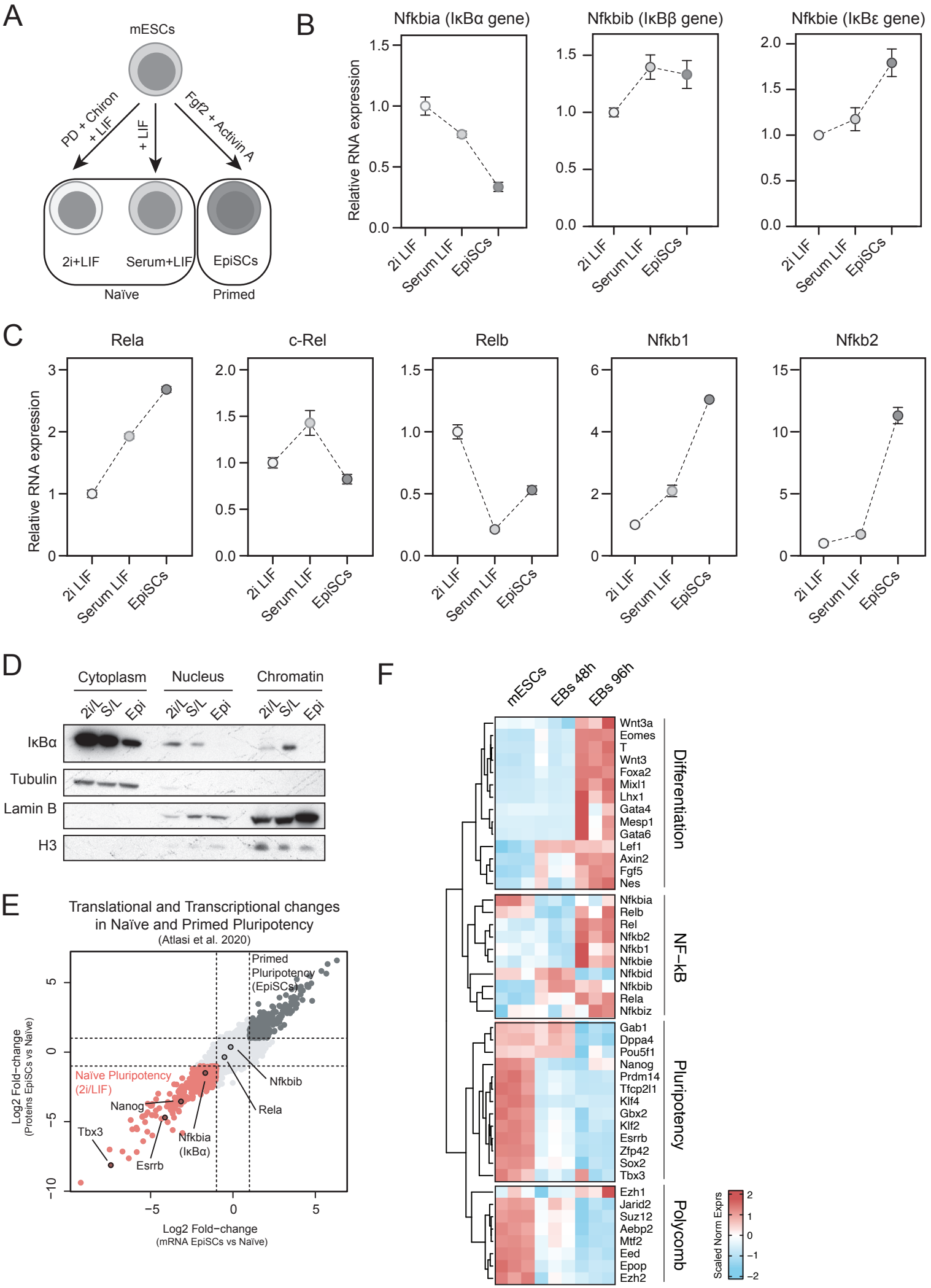
A
mESCs
PD + Chiron + LIF
+ LIF
Fgf2 + Activin A
2i+LIF
Serum+LIF
EpiSCs
Naïve
Primed
B
Nfkbia (IκBα gene)
Nfkbib (IκBβ gene)
Nfkbie (IκBε gene)
Relative RNA expression
2i LIF
Serum LIF
EpiSCs
C
Rela
c-Rel
Relb
Nfkb1
Nfkb2
Relative RNA expression
2i LIF
Serum LIF
EpiSCs
D
Cytoplasm
Nucleus
Chromatin
2i/L
S/L
Epi
IκBα
Tubulin
Lamin B
H3
E
Translational and Transcriptional changes in Naïve and Primed Pluripotency
(Atlasi et al. 2020)
Primed Pluripotency (EpiSCs)
Naïve Pluripotency (2i/LIF)
Nfkbib
Rela
Nanog
Tbx3
Nfkbia (IκBα)
Esrrb
Log2 Fold-change (Proteins EpiSCs vs Naïve)
Log2 Fold-change (mRNA EpiSCs vs Naïve)
F
mESCs
EBs 48h
EBs 96h
Wnt3a
Eomes
T
Wnt3
Foxa2
Mixl1
Lhx1
Gata4
Mesp1
Gata6
Lef1
Axin2
Fgf5
Nes
Differentiation
Nfkbia
Relb
Rel
Nfkb2
Nfkb1
Nfkbie
Nfkbid
Nfkbib
Rela
Nfkbiz
NF-kB
Gab1
Dppa4
Pou5f1
Nanog
Prdm14
Tfcp2l1
Klf4
Gbx2
Klf2
Esrrb
Zfp42
Sox2
Tbx3
Pluripotency
Ezh1
Jarid2
Suz12
Aebp2
Mtf2
Eed
Epop
Ezh2
Polycomb
Scaled Norm Exprs

Figure 2

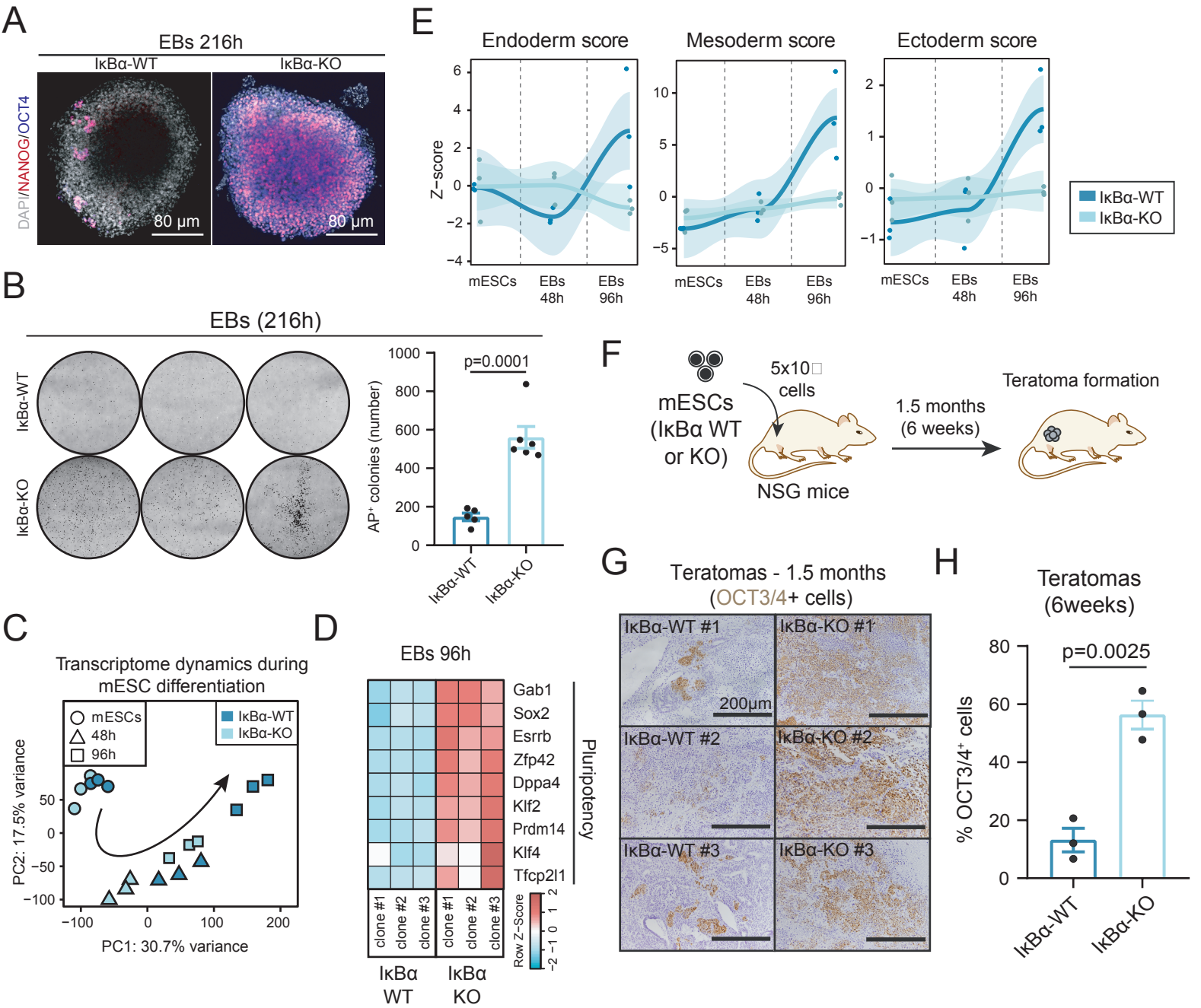
A
EBs 216h
IκBα-WT
IκBα-KO
DAPI/NANOG/OCT4
80 µm
80 µm
B
EBs (216h)
IκBα-WT
IκBα-KO
p=0.0001
AP⁺ colonies (number)
1000
800
600
400
200
0
IκBα-WT
IκBα-KO
C
Transcriptome dynamics during mESC differentiation
mESCs
48h
96h
IκBα-WT
IκBα-KO
PC2: 17.5% variance
PC1: 30.7% variance
50
0
−50
−100
−100
0
100
200
D
EBs 96h
Gab1
Sox2
Esrrb
Zfp42
Dppa4
Klf2
Prdm14
Klf4
Tfcp2l1
Pluripotency
clone #1
clone #2
clone #3
clone #1
clone #2
clone #3
IκBα WT
IκBα KO
Row Z-Score
2
1
0
−1
−2
E
Endoderm score
Mesoderm score
Ectoderm score
Z−score
mESCs
EBs 48h
EBs 96h
IκBα-WT
IκBα-KO
F
mESCs (IκBα WT or KO)
5x10□ cells
NSG mice
1.5 months (6 weeks)
Teratoma formation
G
Teratomas - 1.5 months (OCT3/4+ cells)
IκBα-WT #1
IκBα-KO #1
IκBα-WT #2
IκBα-KO #2
IκBα-WT #3
IκBα-KO #3
200µm
H
Teratomas (6weeks)
p=0.0025
% OCT3/4⁺ cells
80
60
40
20
0
IκBα-WT
IκBα-KO

Figure 3

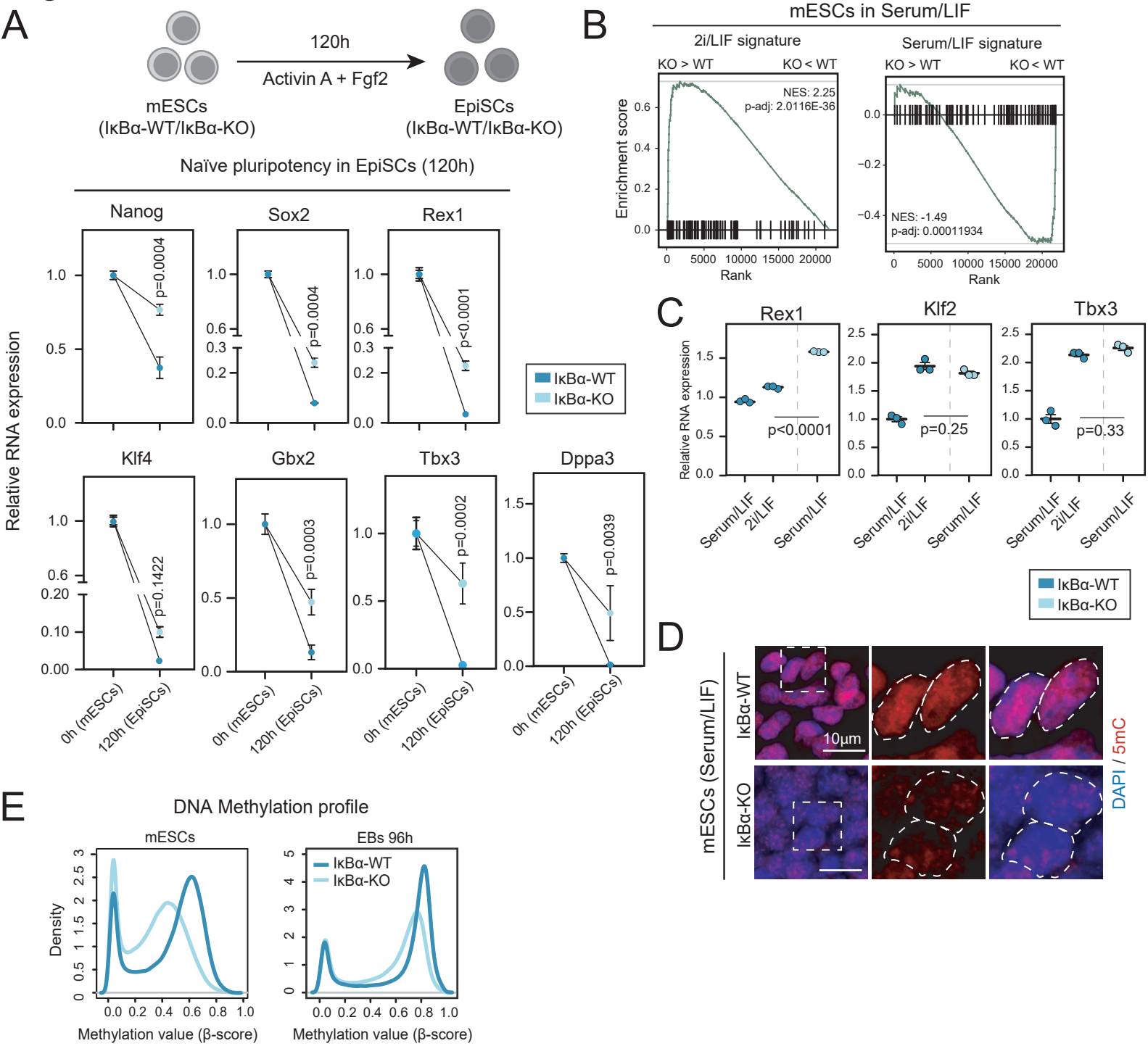
A
120h
Activin A + Fgf2
mESCs
(IκBα-WT/IκBα-KO)
EpiSCs
(IκBα-WT/IκBα-KO)
Naïve pluripotency in EpiSCs (120h)
Nanog
Sox2
Rex1
Klf4
Gbx2
Tbx3
Dppa3
Relative RNA expression
p=0.0004
p=0.0004
p<0.0001
p=0.1422
p=0.0003
p=0.0002
p=0.0039
0h (mESCs)
120h (EpiSCs)
IκBα-WT
IκBα-KO
B
mESCs in Serum/LIF
2i/LIF signature
Serum/LIF signature
KO > WT
KO < WT
NES: 2.25
p-adj: 2.0116E-36
NES: -1.49
p-adj: 0.00011934
Enrichment score
Rank
C
Rex1
Klf2
Tbx3
Relative RNA expression
p<0.0001
p=0.25
p=0.33
Serum/LIF
2i/LIF
Serum/LIF
IκBα-WT
IκBα-KO
D
mESCs (Serum/LIF)
IκBα-WT
IκBα-KO
10μm
DAPI / 5mC

E
DNA Methylation profile
mESCs
EBs 96h
Density
IκBα-WT
IκBα-KO
Methylation value (β-score)

Figure 4

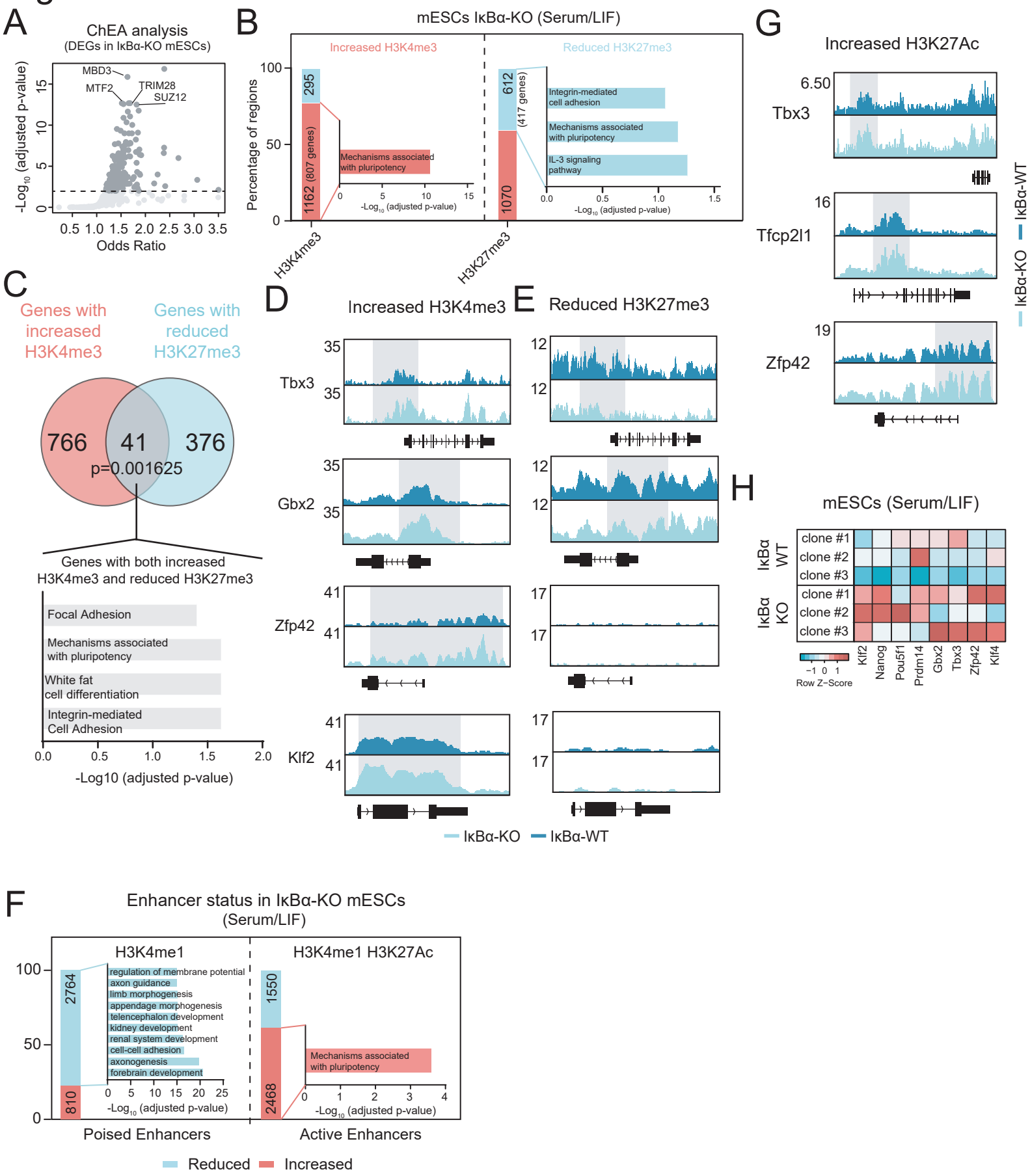
A
ChEA analysis
(DEGs in IκBα-KO mESCs)
MBD3
MTF2
TRIM28
SUZ12
-Log10 (adjusted p-value)
Odds Ratio
B
mESCs IκBα-KO (Serum/LIF)
Increased H3K4me3
Reduced H3K27me3
Percentage of regions
295
1162 (807 genes)
612
(417 genes)
1070
Mechanisms associated with pluripotency
Integrin-mediated cell adhesion
Mechanisms associated with pluripotency
IL-3 signaling pathway
-Log10 (adjusted p-value)
H3K4me3
H3K27me3
C
Genes with increased H3K4me3
Genes with reduced H3K27me3
766
41
376
p=0.001625
Genes with both increased H3K4me3 and reduced H3K27me3
Focal Adhesion
Mechanisms associated with pluripotency
White fat cell differentiation
Integrin-mediated Cell Adhesion
-Log10 (adjusted p-value)
D
Increased H3K4me3
E
Reduced H3K27me3
Tbx3
Gbx2
Zfp42
Klf2
IκBα-KO
IκBα-WT
G
Increased H3K27Ac
Tbx3
Tfcp2l1
Zfp42
IκBα-KO
IκBα-WT
H
mESCs (Serum/LIF)
IκBα WT
IκBα KO
clone #1
clone #2
clone #3
Klf2
Nanog
Pou5f1
Prdm14
Gbx2
Tbx3
Zfp42
Klf4
Row Z-Score
F
Enhancer status in IκBα-KO mESCs
(Serum/LIF)
H3K4me1
H3K4me1 H3K27Ac
2764
810
1550
2468
regulation of membrane potential
axon guidance
limb morphogenesis
appendage morphogenesis
telencephalon development
kidney development
renal system development
cell-cell adhesion
axonogenesis
forebrain development
Mechanisms associated with pluripotency
-Log10 (adjusted p-value)
Poised Enhancers
Active Enhancers
Reduced
Increased

Figure 5

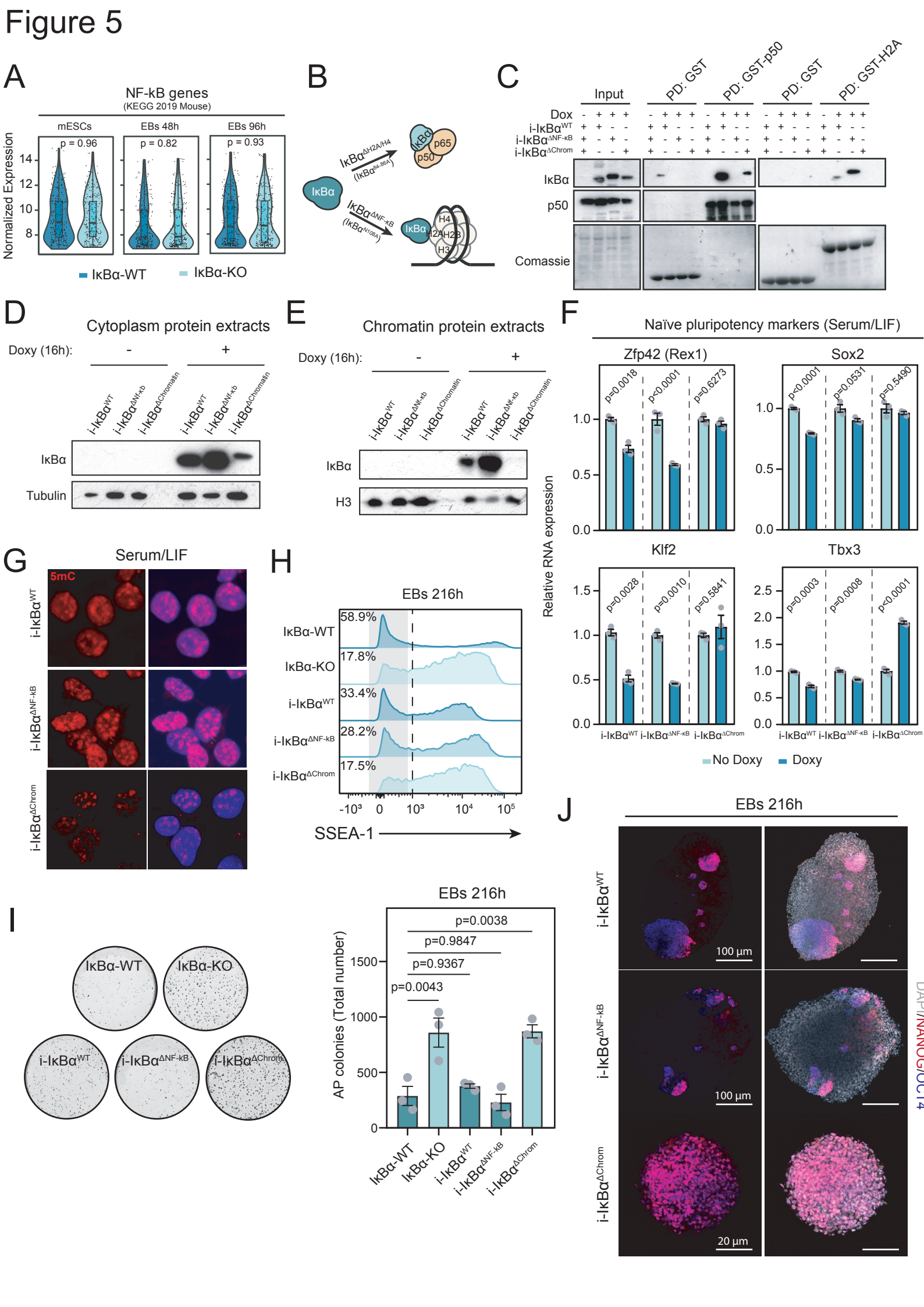
A
NF-kB genes
(KEGG 2019 Mouse)
mESCs
EBs 48h
EBs 96h
p = 0.96
p = 0.82
p = 0.93
Normalized Expression
IκBα-WT
IκBα-KO
B
IκBα
p65
p50
H4
H2A
H2B
H3
C
Input
PD: GST
PD: GST-p50
PD: GST
PD: GST-H2A
Dox
i-IκBα^WT
i-IκBα^ΔNF-κB
i-IκBα^ΔChrom
IκBα
p50
Comassie
D
Cytoplasm protein extracts
Doxy (16h):
Tubulin
E
Chromatin protein extracts
H3
F
Naïve pluripotency markers (Serum/LIF)
Zfp42 (Rex1)
Sox2
Klf2
Tbx3
Relative RNA expression
No Doxy
Doxy
G
Serum/LIF
5mC
H
EBs 216h
58.9%
17.8%
33.4%
28.2%
17.5%
SSEA-1
I
EBs 216h
AP colonies (Total number)
p=0.0038
p=0.9847
p=0.9367
p=0.0043
J
EBs 216h
100 µm
20 µm
DAPI/NANOG/OCT4